Volume 43, Number 1, 2009

A forum for the exchange of circuits, systems, and software for real-world signal processing

Analog Dialogue

In This Issue

2 Editors' Notes; New Product Introductions

3 Smart Metering Technology Promotes Energy Efficiency for a Greener World

6 Equalization and Pre-Emphasis Enable Use of 30-m Cat-5 UTP Cable

9 Low-Cost Video Multiplexing Using High-Speed Amplifiers

11 Using MEMS Accelerometers as Acoustic Pickups in Musical Instruments

15 Power Boost Circuit with Current Sense and Kelvin Connection

17 Analog Microcontroller Forms Heart of Low-Cost, High-Efficiency PA Monitor

21 Reconstruct a DAC Transfer Function from Its Harmonic Spectral Content

25 Notch Filter Reduces Amplifier Peaking and Increases Gain Flatness

27 This Should Work: Thermistor Senses Liquid Levels

www.analog.com/analogdialogue

ANALOG DEVICES

Editors' Notes

IN THIS ISSUE

Smart Metering Technology Promotes Energy Efficiency for a Greener World
We're all familiar with the electricity meter in the garage or basement. We may even have looked at it once or twice to phone an up-to-date reading to the utility company in place of an estimate. Thanks to technology, a quiet revolution is taking place inside this innocuous looking meter. This article describes how automatic meter reading and the smart grid can help improve energy efficiency and reduce carbon emissions. Page 3.

Equalization and Pre-Emphasis Enable Use of 30-m Cat-5 UTP Cable
The use of the category-5 unshielded twisted-pair cable has grown due to its respectable performance and low cost. Currently being used for keyboard-video-mouse networking, this type of cable provides an inexpensive solution for connecting HDTV components when long-distance connectivity is required. Page 6.

Low-Cost Video Multiplexing Using High-Speed Amplifiers
The large number of video sources connected to a single display makes video switching a requirement in home and automotive entertainment systems. In the home, the set-top box, DVR, VCR, DVD player, video game, and PC all feed one display. In cars, the rearview camera, DVD player, navigation system, and auxiliary devices all feed the display. Page 9.

Using MEMS Accelerometers as Acoustic Pickups in Musical Instruments
MEMS microphones have begun to dominate the broad consumer market, including cell phones, Bluetooth headsets, personal computers, and digital cameras. Now, key technologies used in MEMS accelerometers can bring a new dimension to acoustic transducers. Low-*g* accelerometers don't suffer from traditional feedback problems, and show clear potential as high-quality acoustic pickups for musical instruments. Page 11.

Power Boost Circuit with Current Sense and Kelvin Connection
In automatic test equipment, low-current adjustable and high-current fixed voltage sources are available. An additional supply must be created when a high-current adjustable voltage source is required. This article shows how a high-current rail-to-rail op amp boosts the current of an adjustable voltage source. Page 15.

Analog Microcontroller Forms Heart of Low-Cost, High-Efficiency PA Monitor
Saving energy is crucial for efficient wireless network operation. Power amplifiers (PA), the core of base stations and repeaters, can account for more than half of their total power consumption. Monitoring and controlling the PA can improve efficiency and reduce operating costs, maximize output power and achieve the highest possible linearity, and allow the system operator to discover problems and improve reliability. Page 17.

Reconstruct a DAC Transfer Function from its Harmonic Spectral Content
DAC output spectrums contain harmonic content due to their nonideal transient and static behavior. This article defines a method for deriving the DAC transfer function from the observed harmonic content, assuming that the static errors, rather than the transient characteristics, are the dominant source of the distortion. Page 21.

Notch Filter Reduces Amplifier Peaking and Increases Gain Flatness
Although the ADA4817 is unity-gain stable, a high-frequency pole increases its GWP from 410 MHz at high gains to 1 GHz at unity gain, while decreasing its phase margin. Adding a discrete RLC notch filter maintains the high bandwidth and input impedance, while dramatically reducing peaking, increasing gain flatness, and reducing overshoot. Page 25.

This Should Work: Thermistor Senses Liquid Levels
In precision temperature measurement applications using thermistors, RTDs, or other resistive temperature sensors, care must be taken to avoid self-heating errors caused by the excitation current. In some applications, however, the self-heating effect can be put to good use. The design concept presented here should work, but it has not been fully tested. Page 27.

Dan Sheingold [dan.sheingold@analog.com]

Scott Wayne [scott.wayne@analog.com]

PRODUCT INTRODUCTIONS: VOLUME 43, NUMBER 1

Data sheets for all ADI products can be found by entering the part number in the search box at www.analog.com.

January

Amplifier, instrumentation, precision **AD8295**
Amplifier, operational, high-speed triple **ADA4855-3**
Amplifier, operational, high-speed triple **ADA4858-3**
Amplifiers, operational, low-noise single and dual **ADA4817-1/ADA4817-2**
Amplifiers, operational, precision single and dual **ADA4004-1/ADA4004-2**
Amplifier, video, high-speed triple **ADA4856-3**
Amplifier, video, high-speed triple **ADA4859-3**
ADC, pipelined, 11-bit, 200-MSPS **AD9230-11**
ADC, pipelined, quad, 12-bit, 170-MSPS/210-MSPS/250-MSPS ... **AD9239**
Codec, high-definition audio **AD1989B**
Converters, dc-to-dc, 600-mA/1000-mA **ADP2503/ADP2504**
DAC, current-output, 10-bit, 120-mA **AD5398A**
DACs, voltage-output, dual, 12-/14-/16-bit **AD5722/AD5732/AD5752**
Detector, crest-factor, 450-MHz to 6000-MHz **ADL5502**
Driver, line, dual VDSL/VDSL2 ..... **AD8398A**
Drivers, differential ADC, ultralow-distortion .. **ADA4927-1/ADA4927-2**
Energy Meters, single-phase **ADE5166/ADE5169**
Regulators, LDO, adjustable-output, 0.8 A/1.2 A/2.0 A **ADP1753/ADP1755/ADP1741**
Regulators, LDO, fixed-output, 0.8 A/1.2 A/2.0 A **ADP1752/ADP1754/ADP1740**
Regulators, low-dropout, dual, 200 mA **ADP220/ADP221**
Sensor, inertial, four-degrees-of-freedom **ADIS16300**
Synthesizer, PLL, wideband, integrated VCO **ADF4350**

February

DAC, voltage-output, dual, 16-bit **AD5762R**
DACs, voltage-output, dual, 12-/14-/16-bit **AD5722R/AD5732R/AD5752R**
Driver, MOSFET, dual, 12-V **ADP3650**
Energy Meters, single-phase **ADE7116/ADE7156**
Expander, keypad I/O **ADP5588**
Sensor, inertial, six-degrees-of-freedom **ADIS16364**
Signal Processor, HD image, dual, 14-bit **AD9978A**
Switch, HDMI/DVI, 4:1 ..... **ADV3002**
Transceiver, RS-485, 16-Mbps, full-duplex **ADM1491E**

March

Accelerometer, high-performance, wideband **ADXL001**
Accelerometer, low-power, 3-axis, ±3-*g* **ADXL335**
Amplifier, difference, programmable-gain **AD8271**
Amplifier, instrumentation, wide supply range **AD8226**
Amplifier, operational, dual, 1-MHz **ADA4665-2**
ADC, successive-approximation, 16-bit, 6-MSPS **AD7625**
Clock- and Data Recovery, multirate **ADN2855**
Codec, audio, stereo, 24-bit, 96-kHz **ADAU1361**
Codec, audio, stereo, 24-bit, 96-kHz **ADAU1761**
Controller, programmable capacitance sensor **AD7147A**
DAC, current-output, 14-bit, 2500-MSPS **AD9739**
DACs, voltage-output, dual and quad, 16-bit **AD5763/AD5765**
DACs, voltage-output, quad, 14-/16-bit **AD5734R/AD5754R**
Digitizer, video/graphics, 12-bit, 170-MHz **ADV7604**
Driver, laser diode, 11.3-Gbps **ADN2526**
Drivers, line, single and dual LVDS **ADN4661/ADN4663**
Energy Meter, single-phase **ADE7518**
Modulator, quadrature, 50 MHz to 2200 MHz **ADL5386**
Processor, digital audio **ADAU1445**
Receivers, line, single and dual LVDS **ADN4662/ADN4664**
Regulators, low-dropout, 300 mA **ADP170/ADP171**
Sensors, inertial, six-degrees-of-freedom **ADIS16360/ADIS16365**
Switch, power, high-side logic-level control **ADP190**

Analog Dialogue

Analog Dialogue, www.analog.com/analogdialogue, the technical magazine of Analog Devices, discusses products, applications, technology, and techniques for analog, digital, and mixed-signal processing. Published continuously for 43 years—starting in 1967—it is currently available in two versions. Monthly editions offer technical articles; timely information including recent application notes, new-product briefs, pre-release products, webinars and tutorials, and published articles; and potpourri, a universe of links to important and relevant information on the Analog Devices website, www.analog.com. Printable quarterly issues feature collections of monthly articles. For history buffs, the *Analog Dialogue* archive includes all regular editions, starting with Volume 1, Number 1 (1967), and three special anniversary issues. If you wish to subscribe, please go to www.analog.com/analogdialogue/subscribe.html. Your comments are always welcome; please send messages to dialogue.editor@analog.com or to *Dan Sheingold*, Editor [dan.sheingold@analog.com] or *Scott Wayne*, Publisher and Managing Editor [scott.wayne@analog.com].

ISSN 0161-3626

Smart Metering Technology Promotes Energy Efficiency for a Greener World

By Austin Harney

INTRODUCTION

We're all familiar with the electricity meter hidden away in the garage, basement, or other out-of-view location. We may even have looked at it once or twice to phone an up-to-date reading to the utility company in place of an estimate. Thanks to technology, a quiet revolution is taking place inside this innocuous looking meter.

Figure 1 shows an example of a traditional *electromechanical meter*—first developed in the late 19th century—that has a spinning disc and a mechanical counter display. This type of meter operates by counting the revolutions of a metal disc that rotates at a speed proportional to the power drawn through the main fuse box. Nearby coils spin the disc by inducing eddy currents and a force proportional to the instantaneous current and voltage. A permanent magnet exerts a damping force on the disc, stopping its spin after power has been removed.

Figure 1. Electromechanical energy meter.

The first step in meter evolution was the replacement of electromechanical meters with *solid-state electronic meters*. Electronic meters measure energy using highly integrated components, such as the ADE516x,[1] ADE556x,[2] ADE716x,[3] ADE756x,[4] and ADE77xx[5] families of energy-measurement ICs.[6] These devices digitize the instantaneous voltage and current via a high-resolution sigma-delta ADC. Computing the product of the voltage and current gives the *instantaneous power* in watts. Integration over time gives energy used, which is usually measured in kilowatt hours (kWh). The energy data is displayed on a liquid-crystal display (LCD), as shown in Figure 2.

Electronic meters offer several benefits. In addition to measuring instantaneous power, they can measure other parameters such as *power factor* and *reactive power*. Data can be measured and stored at specific intervals, allowing the utility to offer price plans based on time-of-day of usage. This allows savvy consumers to save money by running major appliances, such as washers and dryers, during lower-cost, off-peak periods; and utility companies can avoid building new power plants because less capacity is required during peak periods. Electronic meters are not influenced by external magnets or orientation of the meter itself, so they are more tamper-proof than electromechanical meters. Electronic meters are also highly reliable.

Analog Devices has been a key player in the transition from electromechanical meters to electronic ones, shipping more than 225 million energy measurement ICs to date. According to IMS Research, 75% of all energy meters shipped in 2007 were electronic rather than electromechanical.[7]

Figure 2. Solid-state electronic energy meter.

Electronic Meter Opens Up New Possibilities

Once meter data is available in electronic form, it becomes feasible to add communications to the meter, allowing the meter to use *automatic meter reading* (AMR) to access data remotely via the communication link. Meter manufacturers have developed different system architectures for remote reading, broadly classified as walk-by, drive-by, or networked systems. A drive-by system is shown in Figure 3. In this case, the utility company sends out a van with an on-board wireless data collector. The van drives through the neighborhood efficiently collecting meter data. A drive-by system improves the number of meters a utility employee can read in a day fivefold compared to walk-by systems and over tenfold compared to manual meter reading. In a networked system, meter data is fed to a fixed data collector, which is typically located on a pole at the end of the street or neighborhood. The data is fed back to the utility via a broadband or cellular backbone.

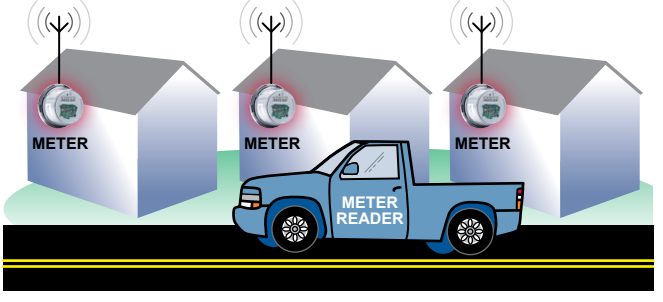

Figure 3. Drive-by meter reader.

AMR to AMI

Initially, replacing manual reading with AMR systems was seen simply as a way to reduce labor costs, but this is changing as the industry recognizes that AMR allows utility companies to conveniently provide higher order benefits and services, such as real-time pricing to promote better energy efficiency, instant reporting of fault detection, and more accurate data for profiling usage within the network. AMR is sometimes replaced with *Advanced Metering Infrastructure* (AMI) to highlight the evolution from simple remote meter reading. AMI networked metering systems can be implemented using technologies ranging from satellites to low-cost radios. The two dominant emerging technologies are RF—using the unlicensed industrial, scientific, and medical (ISM) band—and power-line carrier (PLC).

RF technology uses low-power, low-cost radios to wirelessly transmit the meter information, whereas PLC uses the power line itself. Analog Devices has developed solutions for both of these technologies, with the ADF7xxx family of short-range transceivers[8] addressing the ISM band RF segment and the SALEM® family based on the popular Blackfin® processor[9] addressing the PLC segment. Each of these technologies has its pros and cons. For

water and gas meters in particular, RF technology is becoming the dominant choice due to the safety concerns of having power mains near water or gas. Water meters also have the added complication of often being buried underground. With electricity meters, a combination of both approaches is looking most likely, with North America favoring RF and Europe favoring power line. In the U.S., a small number of houses are typically tied to a single transformer, making PLC less economical. In some implementations, utility companies are deploying AMI using a blend, with power line used to communicate from the data collector to the electricity meter and RF used between the electricity meter and other in-home meters or devices. An interesting Google Maps page highlighting worldwide AMR/AMI deployments[10] and field-trials shows up-to-date information.

Designing the RF Piece of an AMR/AMI-Enabled Utility Meter

Utility meters are often located in or around homes that have an ever-increasing number of wireless devices, so ensuring reliable radio communication is a challenge. High performance from the RF circuitry is required to reject large unwanted signals from devices such as a wireless LAN while decoding the wanted signal that might be as low as fractions of a microvolt at the input to the radio.

Good radio sensitivity is also required because this translates into longer signal transmission ranges. Remember that the meter can be located in a basement or, even worse, underground—yet it needs to communicate with a radio on a pole some blocks away or with a utility van on the street. The lower the sensitivity, the closer the receiving radio needs to be to decode the messages correctly. For a mobile drive-by system, this simply means the van must drive closer to your house, but fixed network infrastructure must use smaller cells and a corresponding larger number of data collectors. High sensitivity will thus minimize network infrastructure costs.

Low power consumption is critical in battery-powered gas and water meters. Meter vendors often try to reduce power consumption in an energy meter because this allows them to port the same design to a water or gas meter. Also, in order to operate in the unlicensed portion of the spectrum, the communication protocol used by the meter and reader must comply with the radio emissions regulations in the country of operation. Several unlicensed bands exist worldwide, the most common ones being at 900 MHz, 2.4 GHz, and 5.8 GHz.

A majority of meter manufacturers have chosen radios in the 900 MHz bands for the links between meters, and between meter and data collector. Radios at these frequencies offer better communication range for a given power budget than competing 2.4-GHz technologies and, thus, allow much wider cell coverage for a given base station or data collector. From the utility's perspective, however, a drawback of using this frequency band has been the lack of available standards. The sub-GHz bands are clearly the best technology choice for battery-powered gas and water meters, inspiring increasing demand for standardization to allow interoperability between different manufacturers' systems. Wireless M-Bus, which has grown out of the wired M-Bus users group, is one example of a standard for communication between meters, and between meter and data collector. M-Bus[11] is now part of the EN European Normative standard detailed in EN 13757. The Wireless M-Bus protocol is detailed in the EN 13757-4 variant. Other standardization efforts at 900 MHz are also underway.

The ADF7020[12] and the soon-to-be-released ADF7023 transceivers are examples of 900-MHz radios that are designed with metering in mind. Both devices are also suitable for systems that must comply with the Wireless M-Bus standard. A block diagram of the ADF7020 is shown in Figure 4.

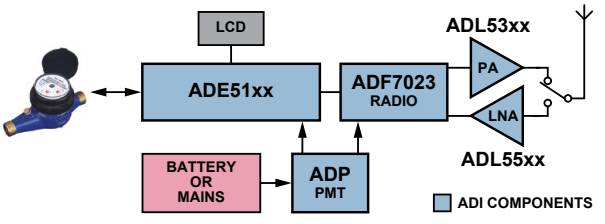

Figure 5. AMR-enabled utility meter.

The ADF7020 fully integrated, low-power radio transceiver operates in the license-free ISM bands at 433 MHz in China, 868 MHz in Europe, and 915 MHz in North America. It integrates the full *transmit* and *receive* RF sections as well as analog and digital basebands. Implementing a radio card for an AMR-enabled utility meter[13] typically requires the ADF7020, an antenna, a small number of external passives, and a simple microcontroller to run the communication protocol, as shown in Figure 5. The ADF7020 significantly eases the burden of the external microcontroller by integrating an ultralow-power, 8-bit RISC core to run some of the lower-level communication functions. This can eliminate the

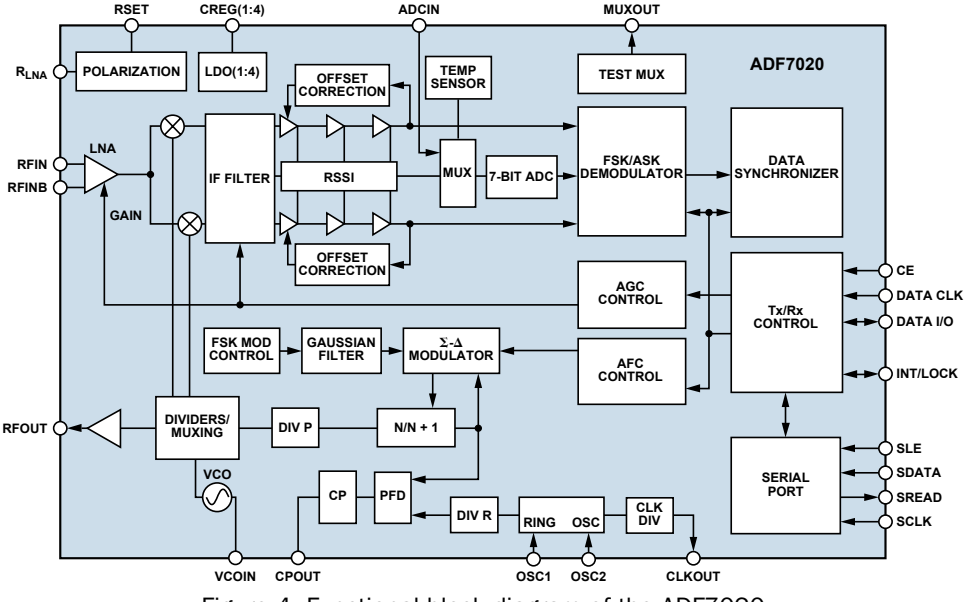

Figure 4. Functional block diagram of the ADF7020.

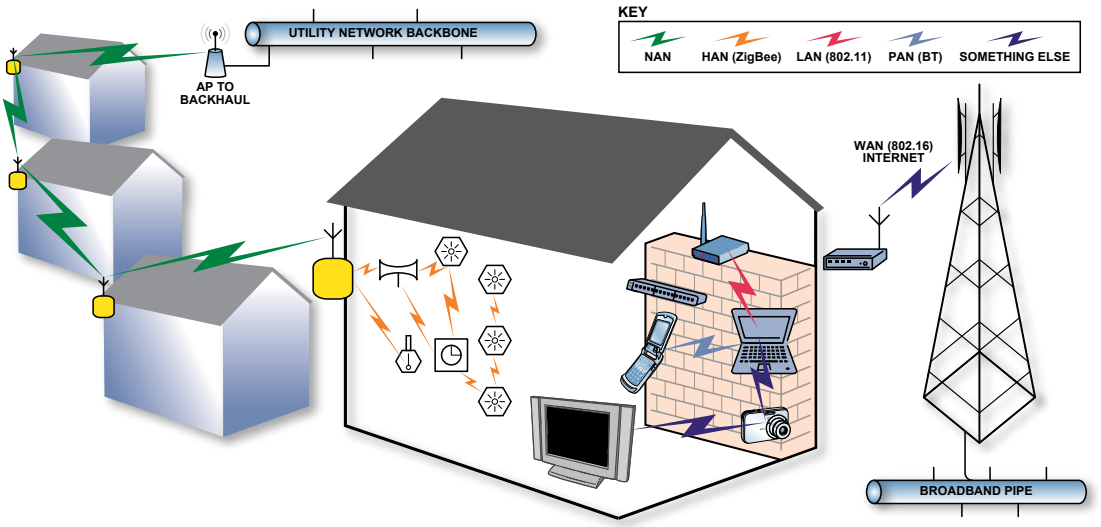

Figure 6. Home area network.

need for a separate communications-specific microcontroller in many cases. Meter manufacturers are also choosing the ADF702x family over competitive parts because their radios offer best-in-class sensitivity and blocking performance, resulting in better range between meter and data collector. The ADF7020 offers blocking performance in excess of 70 dB, meaning that the wanted signal can be detected and decoded correctly even when an unwanted out-of-band signal is up to 70 dB higher than the wanted signal. Adjacent-channel rejection is approximately 40 dB, and sensitivity can be as low as –120 dBm depending on the data-rate. This is more than 20 dB lower than the best performing ZigBee® solutions.[14]

HAN Network

With a communications-enabled meter soon to be available in many homes, utility companies and energy regulators are looking to the future to see how they can leverage the technology to improve energy conservation and awareness. Using this concept, sometimes called the *smart grid*, utility companies can use networks that will extend all the way into customers' homes to actively manage the transmission load. One such service could provide real-time price information, allowing the consumer to modulate energy usage. At times of peak load, during a heat wave for example, the utility company could send a message to the house, telling homeowners that prices would be going up for the next hour and encouraging them to switch off appliances. This would require an in-home display where such a message could be shown. Going one step further, the utility company could communicate to the devices in your home via the meter, turning up the thermostat or turning off a pool pump, for example. This system would require communication between the meter and the home appliances and is sometimes termed the *home area network* (HAN). 900-MHz radios such as the ADF702x and ZigBee radios are both finding favor here.

Most industry participants recognize that a fully working home area network linked with the advanced meter infrastructure is a number of years away, yet the benefits of such a system mean that many companies are actively involved in developing solutions for home area networks today. A graphical depiction of the home area network is given in Figure 6.

CONCLUSION

Analog Devices is focused on supplying leading-edge technology including RF transceivers, energy measurement chipsets, RF amplifiers, isolation products, and power-line control into the metering market. The ADF702x high performance, fully integrated transceiver is suitable for communications-enabled or AMI-ready meters and allows a compact, robust, low-cost solution for meter manufacturers worldwide.

AMI and the smart grid are seen as key potential technologies to improve energy efficiency, ultimately helping in the goal to reduce carbon emissions. Analog Devices is committed to providing innovative and energy-efficient devices to enable this market and to doing its part in improving energy efficiency and promoting energy conservation in the years ahead.

REFERENCES

[1] www.analog.com/en/analog-to-digital-converters/energy-measurement/ADE5166/products/product.html.
[2] www.analog.com/en/analog-to-digital-converters/energy-measurement/ADE5566/products/product.html.
[3] www.analog.com/ADE7166.
[4] www.analog.com/en/analog-to-digital-converters/energy-measurement/ADE7566/products/product.html.
[5] www.analog.com/en/analog-to-digital-converters/energy-measurement/ADE7751/products/product.html.
[6] www.analog.com/en/analog-to-digital-converters/energy-measurement/products/overview/CU_over_analog_ICs_meter__energy-sensitive_world/resources/fca.html?ref=ASC961.
[7] IMS Research Report 2008.
[8] www.analog.com/en/rfif-components/short-range-transceivers/products/index.html.
[9] www.analog.com/en/embedded-processing-dsp/blackfin/content/index.html.
[10] http://maps.google.com/maps/ms?ie=UTF8&hl=en&msa=0&msid=115519311058367534348.0000011362ac6d7d21187&om=1&ll=43.325178,-4.21875&spn=90,-33.046875&source=embed.
[11] www.m-bus.com.
[12] www.analog.com/ADF7020.
[13] www.analog.com/en/instrumentation-solutions/electronic-energy-meter-lcd-display/applications/index.html.
[14] www.zigbee.org/en/index.asp.

AUTHOR

Austin Harney [austin.harney@analog.com] graduated in 1999 with a BEng from University College, Dublin, Ireland, and joined Analog Devices following graduation. He is currently an applications engineer for the ISM-band wireless product line, based in Limerick. In his spare time, Austin enjoys football, music, and spending time with his daughters.

Equalization and Pre-Emphasis Enable Use of 30-Meter Cat-5 UTP Cable

By Charly El-Khoury

Over the past few years, the use of *category-5* (Cat-5) *unshielded twisted-pair* (UTP) cable has grown due to its respectable performance and low cost. This type of cable is currently used for *keyboard-video-mouse* (KVM) networking, with three out of the four twisted pairs carrying the *red, green, and blue* (RGB) video signals. With high-definition television (HDTV) becoming increasingly popular, this type of cable could provide an inexpensive solution when long-distance connectivity—up to 30 meters—is required.

Because Cat-5 UTP cable is made for economy use, its performance degrades rapidly with longer distances. This article presents two solutions that can reduce the transmission losses when using cables up to 30-m long with HDTV 1080p signals, which require a video bandwidth of about 75 MHz.

Figure 1 shows the magnitude response of a 30-m cable vs. frequency. The loss at 75 MHz is about 6 dB, so 6 dB of high-frequency gain must be applied either before transmission or after reception.

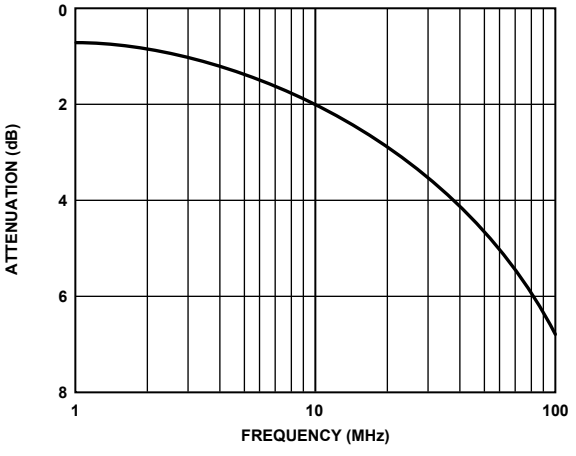

Figure 1. Cable attenuation vs. frequency (30 meters).

Table 1 lists the latest HDTV standards and requirements. High-definition Blu-ray players use 1080p 16:9 HDTV. The exact video bandwidth required is undefined, but 75 MHz should be enough to capture the experience.

Pre-Emphasis

The circuit shown in Figure 2 uses the AD8148[1] driver board with pre-emphasis to compensate for the high-frequency attenuation through a 30-m Cat-5 UTP cable. At the receiver end, the AD8145[2] board—set for a gain of 2— is used without equalization.

Table 1. Common Video Resolutions and Bandwidths

Video Standard	Horizontal Resolution (Pixels/Line)	Vertical Resolution (Lines/ Frame)	Frame Rate (Hz)	Pixel Rate (Mp/s)	Estimated Video BW (MHz)
720p, 16:9 HDTV	1280	720	60	57.6	30
1080i, 16:9 HDTV	1920	1080	30	64.8	32
1080p, 16:9 HDTV	1920	1080	24/30	51.8/ 64.8	32
1080p, 16:9 HDTV	1920	1080	60	130	75

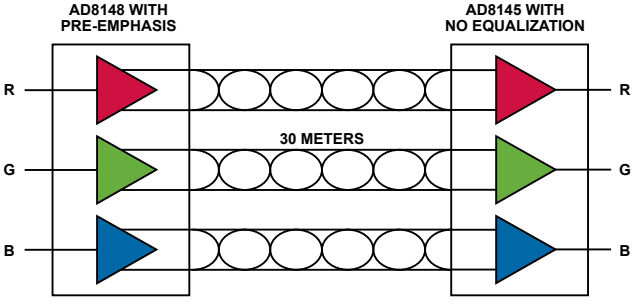

Figure 2. AD8148 with pre-emphasis.

Figure 3 shows the pre-emphasis circuit. The AD8148 differential amplifier is set internally for a gain of 4 (12 dB); the RC network controls the overall gain, which starts with a gain of 2 at low frequencies and slowly increases to a gain for 4 at higher frequencies, as shown in Figure 4.

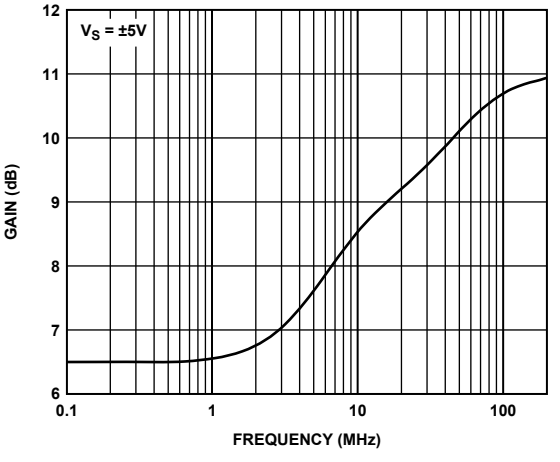

Figure 4. Pre-emphasis gain vs. frequency.

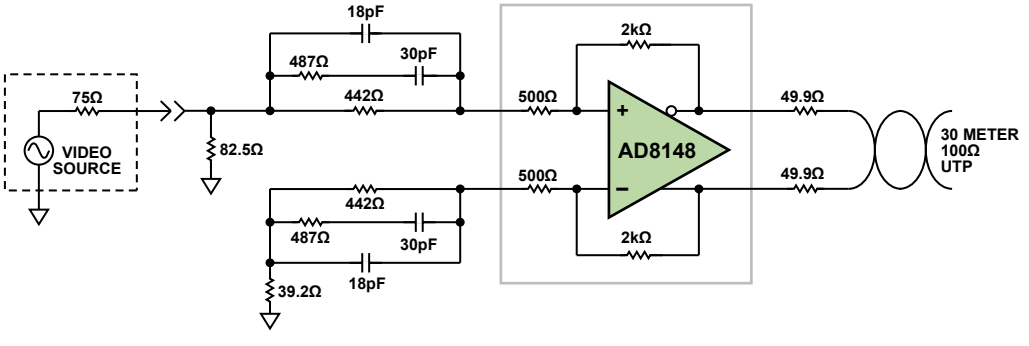

Figure 3. Pre-emphasis circuit.

The general idea is to use the driver's pre-emphasis to counteract the cable's attenuation at high frequencies. Adding the receiver to the output of the cable will not affect the bandwidth, provided the receiver has a flat bandwidth of more than 100 MHz, which is true with an AD8145 set to a gain of 2. Figure 5 shows that the gain at 6 dB is flat to within 1 dB up to 100 MHz, proving that Cat-5 cable can transmit 1080p HDTV.

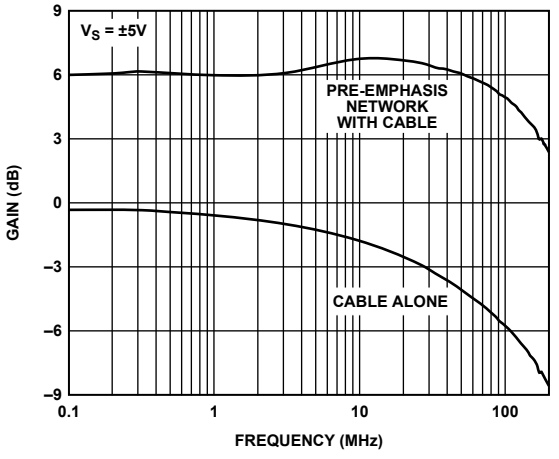

Figure 5. Pre-emphasis network and cable gain vs. frequency.

The performance of this circuit was tested for 10-m, 20-m, and 30-m cable lengths. If a shorter (<5 m) cable is needed, however, the driver can be used without pre-emphasis, as it will be able to handle the shorter distance.

Equalizer

The circuit shown in Figure 6 uses the AD8148 board without pre-emphasis and the AD8143[3] receiver board with equalization. The idea is the same: the high-frequency attenuation of the long cable must be counteracted by boosting the signal gain at higher frequencies. The AD8148 driver is set to a gain of 4; the AD8143 receiver is set to a gain of 1 for low frequencies and a gain of 2 at higher frequencies.

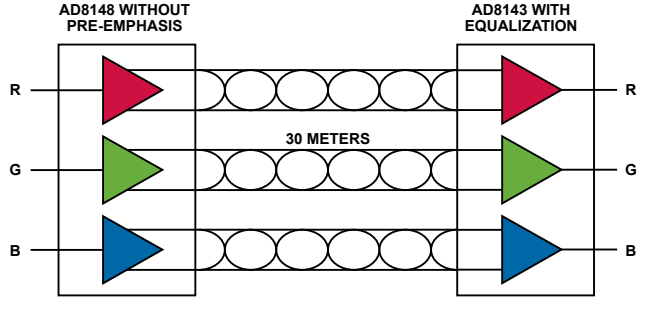

Figure 6. AD8143 with equalization.

Figure 7 shows the equalizer circuit that sets gain at low frequencies to 1 and the gain at high frequencies to 2, as shown in Figure 8. At less than 2 MHz, the gain is 0.5 dB, reaching about 6 dB at 50 MHz.

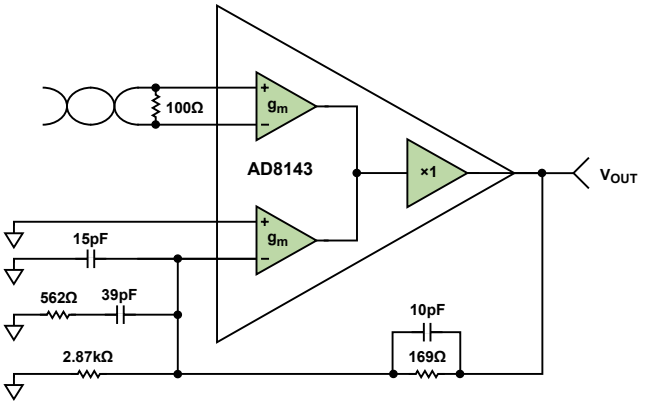

Figure 7. Equalization circuit.

After adding the 30 m cable, the magnitude stays flat to within 1 dB up to 80 MHz, well beyond what is needed for 1080p HDTV. Figure 9 shows about 2-dB peaking at 40 MHz. This will brighten the high-frequency signals a little, but its effect is not noticeable on the screen.

To account for the input and output termination, a gain of 4 is needed. The AD8143 is set at a gain of 1, so the driver must handle a gain of 4 and still have a flat band of more than 100 MHz. At a gain of 4, the AD8148 driver provides a flat response to about 500 MHz, allowing it to support the receiver in 1080p HDTV applications.

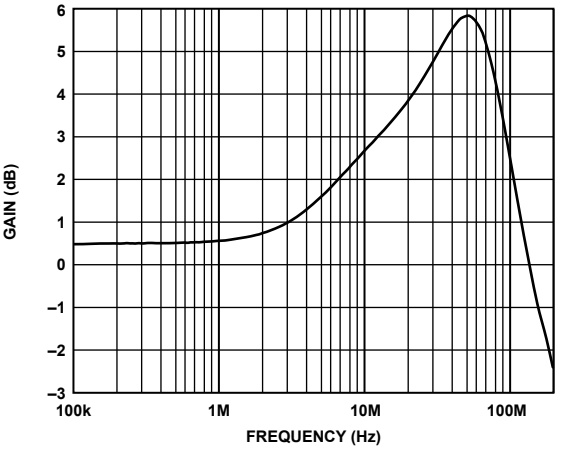

Figure 8. Equalizer magnitude response without cable.

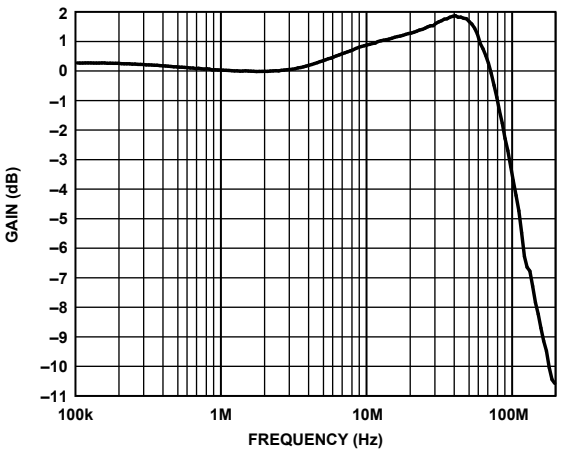

Figure 9. Equalizer magnitude response with the 30 m cable.

Conclusion

The demand for an inexpensive cable that can support HD is rising with the demand for better picture. Cat-5 UTP cable is becoming the best alternative solution. The two solutions proposed for longer distance needs can easily translate to shorter cables by using the AD8148 driver without pre-emphasis along with the AD8145 or AD8143 receivers. In all cases, the proposed solutions always preserve unity gain from the input of the driver to the output of the receiver, with all internal gains compensating for input and output termination losses. These standalone solutions allow inexpensive Cat-5 cable to be used for HD transmission, replacing the more expensive cables on the market today.

References

[1] www.analog.com/en/audiovideo-products/video-ampsbuffersfilters/ad8148/products/product.html.

[2] www.analog.com/en/audiovideo-products/video-ampsbuffersfilters/ad8145/products/product.html.

[3] www.analog.com/en/audiovideo-products/video-ampsbuffersfilters/ad8143/products/product.html.

Pearson, Jonathan. "Adjustable Cable Equalizer Combines Wideband Differential Receiver with Analog Switches." *Analog Dialogue*. Volume 38-07. July 2004.

Budak, Aram. *Passive and Active Network Analysis and Synthesis.* Houghton Mifflin. 1974.

Low-Cost Video Multiplexing Using High-Speed Amplifiers

By Don Nisbett

Over the past few years, the number of video sources connected to a single display has increased steadily, making video signal switching a necessity in most video systems. In a typical home entertainment system, for example, a set-top box (STB) or digital video recorder (DVR) for cable or satellite TV, a VCR, a DVD player, a video game console, and a PC all feed a single display. The ability to switch multiple video sources to a single display extends to cars as well, where video sources include the vehicle entertainment system (VES), rearview camera, DVD player, navigation system, and auxiliary video input.

Traditional CMOS multiplexers and switches suffer several disadvantages at video frequencies—their *on* resistance introduces distortion, degrades differential gain and phase performance, and interacts with the termination resistor to attenuate the incoming video signal and affect the luminance. System designers solve this issue by adding external buffers to add gain and increase drive capability.

Video multiplexing can be simplified by using high-speed video amplifiers with a disable mode. When the amplifier is disabled, its output stage goes into a high-impedance state. This differs from the power-down mode, which significantly lowers the power consumption but leaves the state of the output stage undefined.

High-speed video amplifiers[1] have all the key features required to make them ideal for this function. Their high input impedance does not affect the characteristic impedance of the transmission line, thus allowing back termination. Because they are video amplifiers, they have inherently good video specifications, including differential gain and phase, slew rate, bandwidth, and 0.1-dB flatness.

In a mux configuration, the disabled channels present a high-impedance load to the single active channel. The gain setting and feedback resistors load the active amplifier, but their values are large compared to the 150-Ω video load, so their effect is negligible. Some high-speed video amplifiers that possess these key features are the AD8013, AD8029, and AD8063. Table 1 shows a representative list of muxable video amplifiers.

3:1 Video Multiplexer

The ADA4853-3 has independent disable controls, making it suitable for use as a low-cost 3:1 buffered-output video mux. Its output impedance is greater than 2-kΩ at 10 MHz, so the amplifier outputs can be connected to form a 3:1 mux with excellent switching behavior and great isolation characteristics. Operating on a single 5-V supply, the configuration shown in Figure 1 provides 14-MHz bandwidth (0.1-dB), gain of +2, and 58-dB *off*-channel isolation at 10 MHz. Its 10-µs channel-to-channel switching time supports CVBS analog video applications.

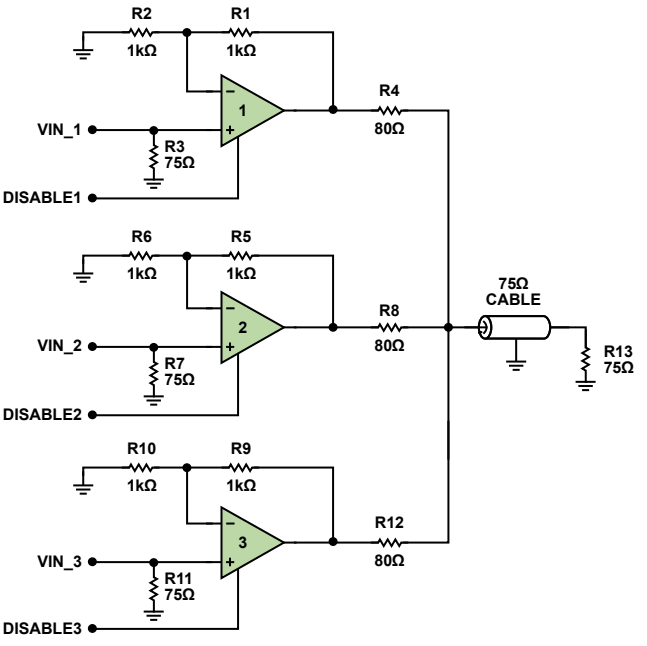

Figure 1. 3:1 video mux.

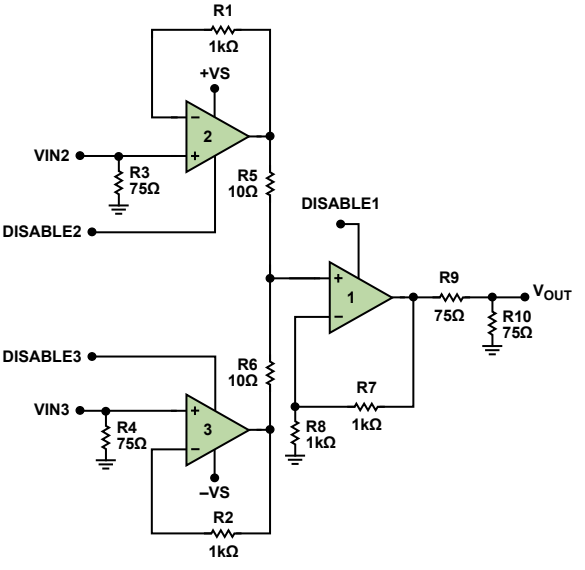

Figure 2. 2:1 video mux.

High-Performance 2:1 Video Multiplexer

Figure 2 shows a high-performance 2:1 mux. The two input amplifiers are configured as unity gain followers, while the output amplifier is set for a gain of +2. The ability to shut down both stages allows this mux to achieve the excellent input-to-output *off*-isolation shown in Figure 3. Switching time in this configuration is 45 µs.

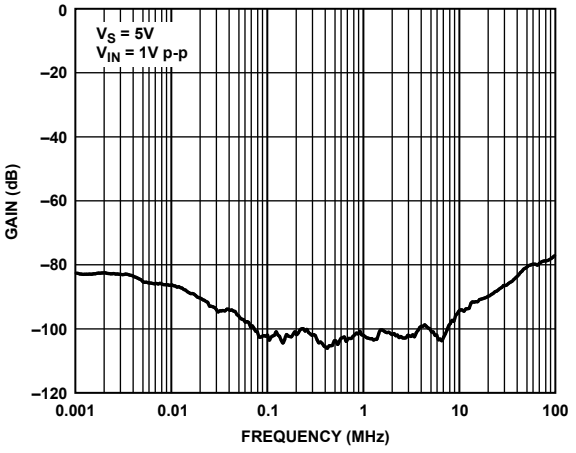

Figure 3. *Off*-isolation of 2:1 mux using the ADA4853-3.

2:1 Video Multiplexer with SAG Correction

Signal amplitude gain (SAG) correction is used to provide low-frequency compensation for the high-pass filter formed by the 150-Ω video load of a back-terminated cable and the output coupling capacitor. Traditional ac-coupling uses a large, expensive coupling capacitor, making it costly and wasting valuable PCB space. SAG correction allows two small, low-cost capacitors to replace the one large ac-coupling capacitor. Figure 4 shows a high-performance 2:1 multiplexer with SAG correction. The compensation network includes C1, C2, R11, and R12. *Field tilt* is a measure of the voltage droop (tilt) that occurs on the ac-coupling capacitor when a constant luma signal is applied. This droop is caused by the small discharge current created by the 75-Ω load resistor. The capacitor values shown are optimized to achieve the equivalent field tilt of a 220-µF ac-coupling capacitor. A typical 220-µF tantalum ac-coupling capacitor occupies 28 mm^2 and costs $0.50 in high volume. The typical 47-µF and 22-µF capacitors used for SAG correction occupy about 0.72 mm^2 and 0.4 mm^2 and cost as little as $0.10 each in high volumes.

Conclusion

High-speed video amplifiers with individual disable pins are excellent for constructing simple, low-cost video multiplexers and switches for composite and high-resolution video. They are ideal for replacing CMOS switches, and are more cost effective than video multiplexers. Be sure to consider using high-speed video amplifiers if your system requires video switching capability.

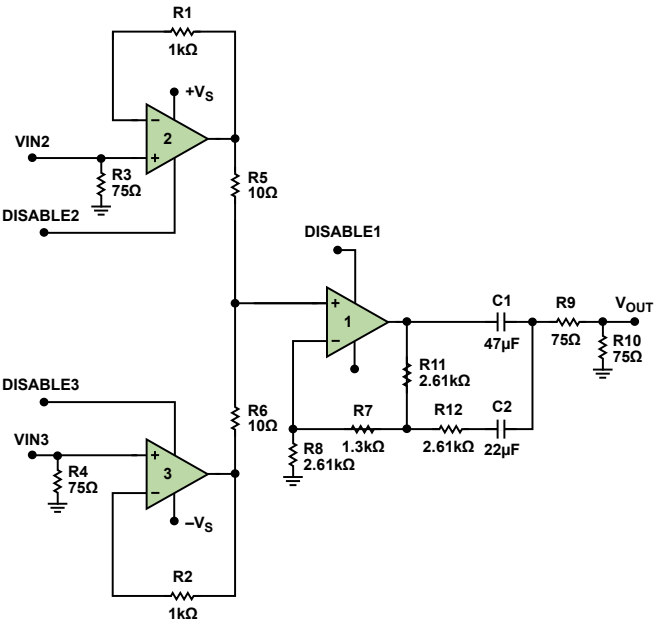

Figure 4. 2:1 video mux.

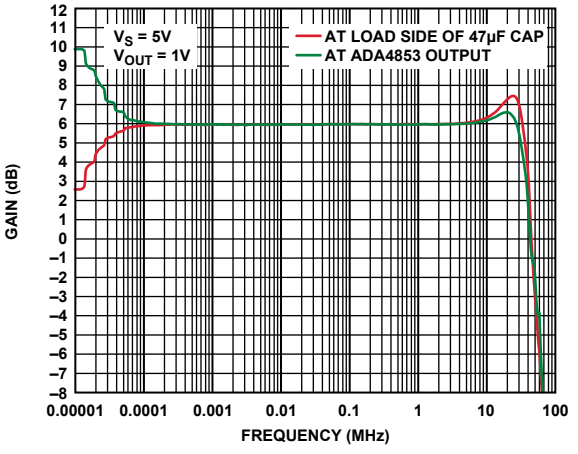

Figure 5. Frequency response of 2:1 mux with SAG correction.

References

[1] www.analog.com/en/amplifiers-and-comparators/video-ampsbuffersfilters/products/index.html#Video_Op-Amps.

Table 1. Muxable High-Speed Amplifiers

Part Number	Number of Amps	–3 dB Bandwidth (MHz)	0.1 dB Flatness (MHz)	Slew Rate (V/µs)	Output Impedance @ 10 MHz (kΩ)	Package
AD8021	Single	490	13	110	2	SOIC, MSOP
AD8027	Single	190	12	100	5	SOIC, SOT-23
AD8029	Single	120	6	55	2	SOT-23, SOIC
AD8063	Single	320	30	650	3.2	SOT-23
AD8099	Single	440	33	715	1.5	SOIC, LFCSP
ADA4853-1	Single	100	22	120	40	SC70
ADA4899-1	Single	535	25	185	1.7	SOIC, LFCSP
ADA4853-2	Dual	100	22	120	40	LFCSP
AD813	Triple	50	20	100	1.5	SOIC
AD8003	Triple	1050	83	2860	1	LFCSP
AD8013	Triple	125	50	400	2	SOIC
AD8023	Triple	125	7	1200	0.6	SOIC, SC70
ADA4853-3	Triple	100	22	120	2	LFCSP, TSSOP

Sonic Nirvana: Using MEMS Accelerometers as Acoustic Pickups in Musical Instruments

By Rob O'Reilly, Alex Khenkin, and Kieran Harney

Introduction

MEMS[1] (microelectromechanical systems) technology builds on the core fabrication infrastructure developed for silicon integrated circuits. Micromechanical structures are created by etching defined patterns on a silicon substrate to form sensor elements or mechanical actuators that can move fractions of a micron. Pressure sensors, one of the first high volume MEMS applications, now monitor pressure in hundreds of millions of engine manifolds and tires; and MEMS accelerometers have been used for over 15 years for airbag deployment, rollover detection, and automotive alarm systems.

MEMS accelerometers[2] are also used for motion sensing in consumer applications, such as video games and cell phones. MEMS micromirror optical actuators are used in overhead projectors, HDTVs, and digital theater presentations. In recent years, MEMS microphones[3] have begun to proliferate the broad consumer market, including cell phones, Bluetooth headsets, personal computers, and digital cameras.

This article describes some of the key technologies deployed in MEMS accelerometer products and discusses how this technology can bring a new dimension to acoustic transducers.

MEMS Accelerometer Technology

The core element of a typical MEMS accelerometer is a moving beam structure composed of two sets of fingers: one set is fixed to a solid ground plane on a substrate; the other set is attached to a known mass mounted on springs that can move in response to an applied acceleration. This applied acceleration (Figure 1) changes the capacitance between the fixed and moving beam fingers.[4]

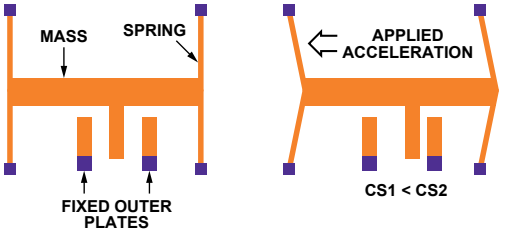

Figure 1. MEMS accelerometer structure.

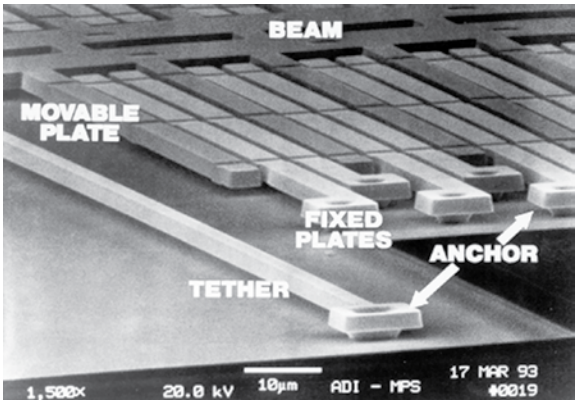

Figure 2. ADXL50 MEMS accelerometer structure.

The dimensions of these MEMS structures, on the order of microns (Figure 2), require very high precision silicon photolithography and etching process technologies. MEMS structures are typically formed from single-crystal silicon, or from polysilicon that is deposited at very high temperatures on the surface of a single-crystal silicon wafer. Structures with very different mechanical characteristics can be created using this flexible technology. One mechanical parameter than can be controlled and varied is spring stiffness. The mass of the sense element and the damping of the structure can also be modified by design. Sensors can be produced to measure fractions of one *g* or hundreds of *g*'s with bandwidths as high as 20 kHz.

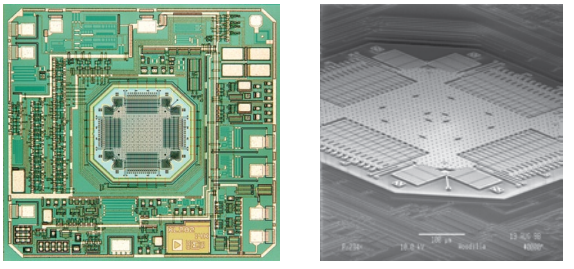

Figure 3. ADXL202 ±2 *g* accelerometer.

The MEMS sensing element can be connected to the conditioning electronics on the same chip (Figure 3) or on a separate chip (Figure 4). For a single-chip solution, the capacitance of the sense element can be as low as 1 to 2 femtofarads per *g*, which equates to measurement resolution in the attofarad range! In a two-chip structure, the capacitance of the MEMS element must be high enough to overcome the parasitic capacitance effects of the bond wires between the MEMS and the conditioning ASIC (application specific integrated circuit).[5]

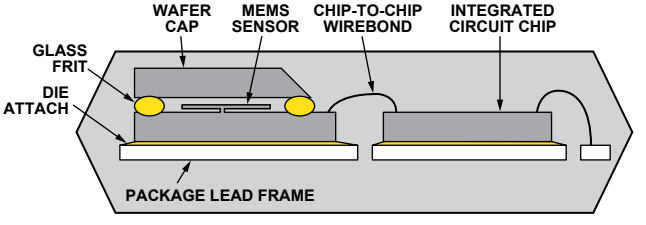

Figure 4. Cross-section of a typical two-chip accelerometer.

Accelerometers as Vibration Measurement Sensors

The concept of using vibration sensing transducers as acoustic pickups in musical instruments is not new.[6] Piezo- and electromagnetic transducers are the basis for many of today's acoustic pickup applications. Tiny MEMS accelerometers are so small and low in mass that they have no mechanical or mass loading effect on the instrument, making them attractive for these applications; but to date their use has been limited due to the narrow bandwidth of commercially available acceleration sensors.

Some recent breakthroughs in accelerometer technology have enabled the production of very small accelerometers with very wide bandwidth. The ADXL001[7] (Figure 5) high-*g* (±70 *g* to ±500 *g*), single-axis accelerometer has 22-kHz bandwidth and comes in a 5-mm × 5-mm × 2-mm package. This is ideal for monitoring vibration to determine the state-of-health of motors and other industrial equipment by detecting changes in their acoustic characteristics. In the early stages of bearing wear, a clear vibration signature that develops in the audio band can be detected with a high-*g* vibration sensor attached to the system housing. This particular sensor, which measures acceleration on the order of 10s of *g*'s, is not sensitive enough for use as an acoustical vibration sensor for musical instruments. Also, it only senses along one axis of motion, while an ideal acoustic sensor will measure the response along all three axes. It does demonstrate, however, that full audio bandwidth acceleration transducers can be produced using MEMS technology.

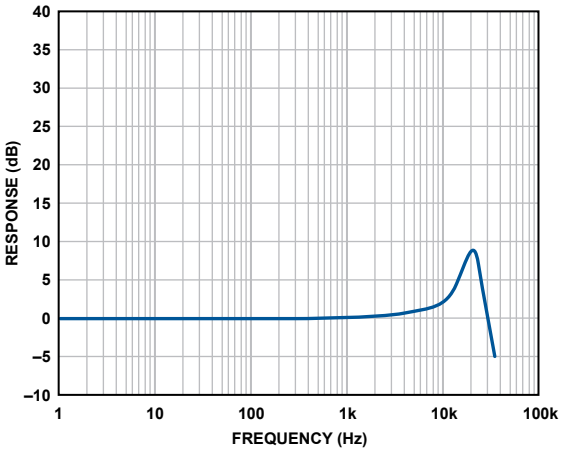

Figure 5. ADXL001 Frequency response curve.

Low-*g* accelerometers can measure acceleration down to milli *g*'s, but are typically bandwidth-limited around 5 kHz. This limitation may be associated with the fact that few commercial applications require significant bandwidth (the primary applications involve the detection of human motion or gravity-driven acceleration), so there has been little motivation to develop sensors suited specifically for audio band measurement.

A 3-axis accelerometer has three separate outputs that measure acceleration along the Cartesian *X*, *Y*, and *Z* axes. The ADXL330[8] 3-axis, low-*g* accelerometer has wider effective bandwidth than other traditional low-*g* accelerometers. Its bandwidth is up to 6 kHz on *X*- and *Y* axes, and around 1 kHz on the *Z* axis. While not ideal, this expanded bandwidth allows the part to gather useful information in the audio band. The output is analog, so it can be easily instrumented and used with standard audio recording equipment. Housed in a standard surface-mount package, it takes advantage of the mature semiconductor manufacturing infrastructure. Measuring less than 4 mm × 4 mm × 1.45 mm (Figure 6), the product can fit into places unimaginable with traditional accelerometer technology. Its very small size does not cause mass loading or other changes in the response of the system being measured. Later we will explore how this low-*g* accelerometer can be applied as an acoustic pickup for a guitar.

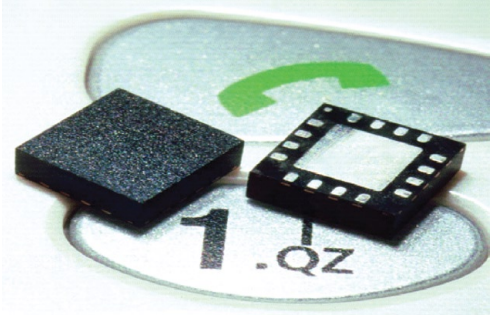

Figure 6. MEMS accelerometer, 4 mm × 4 mm × 1.45 mm.

Acoustic Feedback

Beginning with the introduction of omnidirectional condenser and dynamic microphones in the mid 1920s[9] by Søren Larsen, the Danish scientist who first discovered the principles of audio feedback (known as the Larsen effect), acoustic feedback has been a demon few audio engineers are able to totally control, making it unavoidable in live sound. The Beatles experimented with this audio artifact, then decided to add it to their memorable introduction to "I Feel Fine" in 1964.[10] Rock 'n' Roll then set out to tame the beast by embracing it, making acoustic feedback a striking characteristic of rock music. Electric guitar players such as Pete Townshend and Jimi Hendrix deliberately induced feedback by holding their guitars close to the amplifier. As the fad waned, audio engineers continued their struggle with acoustic feedback's undesirable ear-shattering effects, particularly in live sound applications. In the perfect world of a well-appointed and acoustically treated recording studio, a high-end omnidirectional microphone will record instruments with an astonishing degree of realism and fidelity. Artists who know and cherish this sound have long sought the ability to reproduce it on stage. Although recording a live show with studio sound quality is every musician's dream, it has been virtually impossible. Even if sound reinforcement rigs sounded good, arenas had excellent acoustics, and sound engineers knew everything there was to know about mixing sound and had the best gear available, there would still remain one obstacle on the road to sonic nirvana: feedback.

Acoustic Pickups

Acoustic feedback is typically minimized by using directional microphones. This works to a certain extent, but requires constant management by sound engineers to adapt to the changing characteristics of a stage venue.

Musical instruments can be amplified using pickups. The technologies vary, but the basic idea is to sense the vibrations of the instrument's body directly, rather than the sound it produces in the air. The advantage is obvious: these pickups generate almost no acoustic feedback as they are not sensitive to airborne sound. The shortcomings are many: finding a good-sounding location on an instrument body is notoriously difficult, the sonic characteristics of piezo pickups are far from perfect, and their high output impedance requires special instrument inputs or direct boxes. In addition, they can be large and can interfere with the natural acoustic behavior of the instrument.

This leads to the idea of a low-mass *contact microphone*. Suppose that we used a *surface transducer* that measured the acceleration of the instrument's body, preferably on more than one axis.[11] This transducer would have good linearity and be so lightweight that it would not acoustically affect the instrument being measured. Suppose further that the transducer had similar output level, output impedance, and power requirements as a traditional microphone. In short, suppose that a musician could just plug this transducer into a microphone preamp or mixer input, just like any other microphone.

Contact Microphones

An attentive reader will notice the mention of acceleration in the preceding paragraph. Our ears respond to sound pressure, so microphones are designed to sense sound pressure. To simplify matters greatly, the sound pressure in the immediate vicinity of a vibrating body is proportional to acceleration.[12] What if an accelerometer had enough bandwidth to be used as a contact microphone?

To explore this concept, a 3-axis accelerometer was mounted on an acoustic guitar to act as a pickup. The vibration of the instrument was measured and compared to the built-in piezo pickup and to a MEMS microphone mounted near the guitar. The guitar used was a Fender Stratacoustic acoustic with a built-in Fender pickup. An analog output MEMS accelerometer was mounted on a lightweight flex circuit (Kapton® with etched traces) and attached to the guitar body using beeswax at the bridge location, as shown in Figure 7. The *X*-axis of the accelerometer was oriented along the axis of the strings, the *Y*-axis was perpendicular to the strings, and the *Z*-axis was perpendicular to the surface of the guitar. A MEMS microphone with a flat frequency response out to 15 kHz was mounted 3" from the strings for use as a reference.

Figure 7. Accelerometer mounted on Fender Stratacoustic acoustic guitar.

A short sound segment was recorded using the accelerometer, the built-in piezo pickup, and the MEMS microphone. The time domain waveforms for each transducer are shown in Figure 8. No postprocessing was done on any of the audio clips.

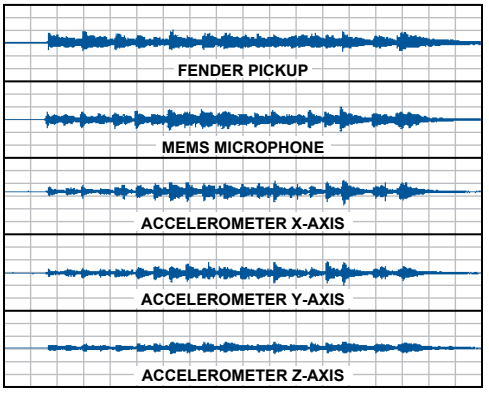

Figure 8. Time domain waveforms using different transducers.

Figure 9 shows an FFT-based spectrum of the piezo pickup measured at one of the peaks in the time domain waveform. This spectrum shows a response with a strong bass component. Indeed, the actual audio file sounded excessively full, with a lot of bass response. This sounds pleasing (depending on your taste), as the cavity resonance creates a fuller bass sound than that heard when listening to the instrument directly.

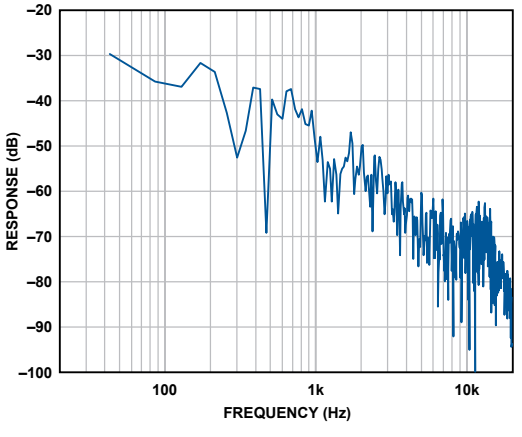

Figure 9. Spectrum of piezo pickup.

The MEMS microphone output is very flat and reproduces the sound of the instrument very well. It sounds very natural, well balanced, and true to life. The FFT-based spectrum measured at the same point in time as the piezo pickup is shown in Figure 10(a). The frequency response of the MEMS microphone is shown in Figure 10(b) for reference.

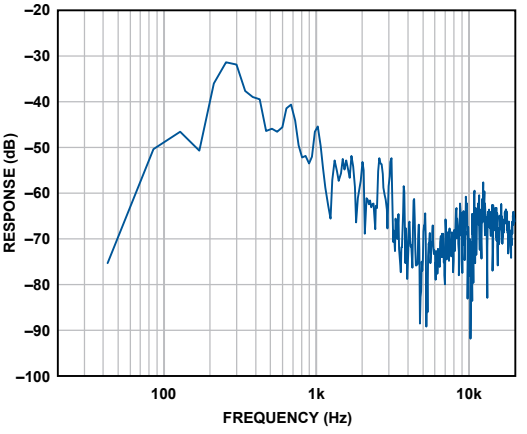

Figure 10(a). Spectrum of MEMS microphone.

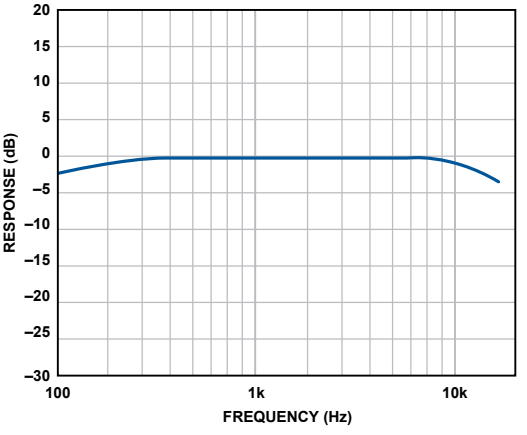

Figure 10(b). Frequency response of MEMS microphone.

The output from the MEMS accelerometer is very interesting. The immediate weak points are that the noise floor was too high and audible at the beginning and end of the track, and that the bandwidth of the *Z*-axis was clearly limited to lower frequencies. The sound reproduction from each axis was noticeably different.

The *X*- and *Y*-axes sounded bright and articulate and had clearly discernible differences in tonality. As expected, the *Z*-axis obviously sounded bass dominated. Figure 11 shows the *X*-axis spectrum (a), the *Y*-axis spectrum (b), and the *Z*-axis spectrum (c).

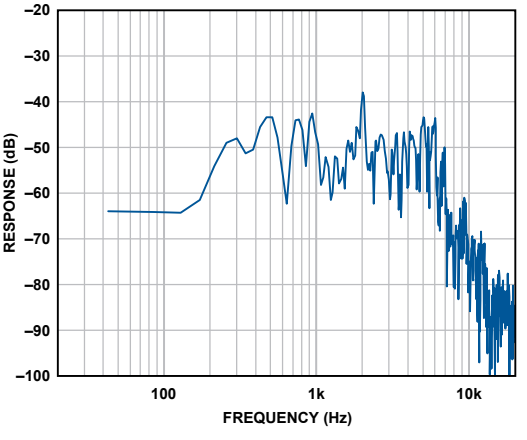

Figure 11(a). Spectrum of *X*-axis.

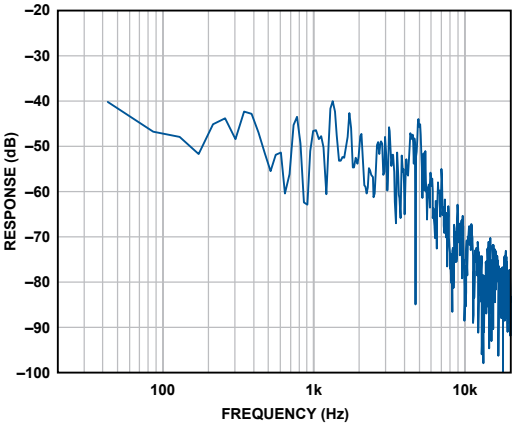

Figure 11(b). Spectrum of *Y*-axis.

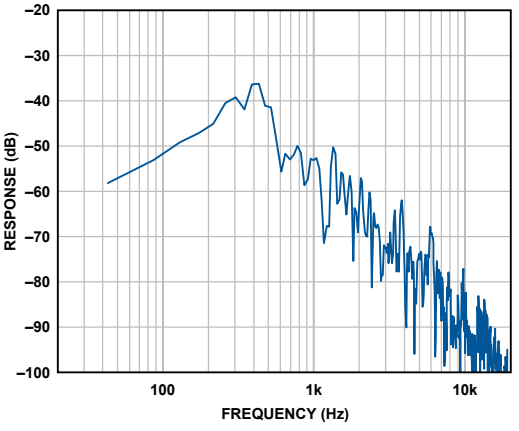

Figure 11(c). Spectrum of *Z*-axis.

The *X*-, *Y*-, and *Z* axes mixed together produced a fair representation of the instrument with some brightness. By adjusting the mix, a variation in tonal balance can be achieved with natural sound reproduction. The extended upper harmonics are still missing due to the bandwidth limitation of the current accelerometers, but the sound reproduction was still surprisingly true.

Conclusion

Low-*g* MEMS accelerometers do not suffer from traditional feedback problems and demonstrate clear potential as high-quality acoustic pickups for musical instruments. A 3-axis accelerometer mounted on a Fender Stratacoustic acoustic guitar achieved promising sound reproduction. The three axes have different tonal characteristics related to the vibration modes of the instrument in the different directions of the body. The three output channels can be mixed to generate realistic sound reproduction. In addition, these channels can be mixed in different ways resulting in creative tonal effects.

While the performance of the accelerometer in this experiment is very promising, there are a few drawbacks. The noise floor of the sensor is audible; a problem that can be minimized using noise gating or other techniques, but the ideal sensor will have a noise floor comparable to conventional microphones. The high frequency response of the sensor needs to be extended, ideally up to 20 kHz to capture the full tonal range of the instrument.

MEMS accelerometer technology has clear potential for acoustic pickup applications in musical instruments, especially in live performances where acoustic feedback could be a problem. A very small, low-power MEMS device can be mounted unobtrusively anywhere on the instrument without affecting its natural vibration characteristics. In fact, multiple sensors can be mounted at different points around the instrument to provide the sound engineer additional flexibility to reproduce the natural character of the instrument without fear of acoustic feedback in live sound application—one step closer to "Sonic Nirvana."

References

[1] www.analog.com/en/mems-and-sensors/products/index.html.

[2] www.analog.com/en/mems-and-sensors/imems-accelerometers/products/index.html.

[3] www.analog.com/en/mems-and-sensors/imems-microphone/products/index.html.

[4] Goodenough, F. "Airbags Boom When IC Accelerometer Sees 50 G." *Electronic Design*. August 8, 1991.

[5] Rai-Choudhury, P. "MEMS and MOEMS Technology and Applications." SPIE Press. 2000.

[6] Hopkin, B. "Getting a Bigger Sound: Pickups and Microphones for Your Musical Instrument." Sharp Press. 2002.

[7] www.analog.com/en/mems-and-sensors/imems-accelerometers/adxl001/products/product.html.

[8] www.analog.com/en/mems-and-sensors/imems-accelerometers/adxl330/products/product.html.

[9] Olsen, H. "A History of High Quality Studio Microphones." *J. of Audio Engineering Society*, 24. December 1976.

[10] Fontenot, R. "I Feel Fine: The History of this Classic Beatles Song." About.com.

[11] Freed, A. and O. Isvan. "Musical Applications of New, Multi-Axis Guitar String Sensors." International Computer Music Conference. pp 543–546. 2000.

[12] Olsen, H. "Acoustical Engineering." Professional Audio Journals Inc. 1991.

Authors

Rob O'Reilly [rob.oreilly@analog.com], who began his career at ADI in 1993, is responsible for future business and product development in the Micromachined Products Division. Rob formerly led the Advanced Test, Test, Trim/Probe, and Characterization groups and, over the past 15 years, has played a key role in the development of *i*MEMS® accelerometer and gyroscope test, reliability, and characterization processes.

Alex Khenkin [alex.khenkin@analog.com] is a senior acoustics engineer at ADI. With over a decade of experience in microphone research and design at Earthworks, Inc., he has worked extensively on extending the frequency response and dynamic range of microphones, paying special attention to their time-domain characteristics. Alex received his master's degree in applied acoustics at Moscow State Institute of Radio-Engineering, Electronics, and Automation (MIREA). In his free time, he enjoys playing classical guitar.

Kieran Harney [kieran.harney@analog.com], a product line manager in the Micromachined Products Division, is focused on the development of new MEMS technologies. He joined ADI 22 years ago as a semiconductor packaging engineer in Limerick, Ireland; served as assembly and test manager in the Philippines from 1994 to 1997; and assumed responsibility for assembly, test, and advanced package development in Cambridge, MA, in 1997. Kieran received a manufacturing engineering degree in 1983 and an MBA in 1993, both from the University of Limerick, Ireland.

Power Boost Circuit with Current Sense and Kelvin Connection

By Angel Caballero and Greg DiSanto

In automatic test equipment[1] (ATE), low-current adjustable voltage sources and high-current fixed voltage sources are available. An additional supply must be created when a high-current adjustable voltage source is required.

This article shows how an AD8397[2] high-current rail-to-rail op amp boosts the current of an adjustable voltage source to up to ±750 mA. The buffered voltage can be used as a power supply or a reference. A Kelvin connection eliminates resistive losses. This technique provides an accurate voltage and allows the current to be measured with a sense resistor.

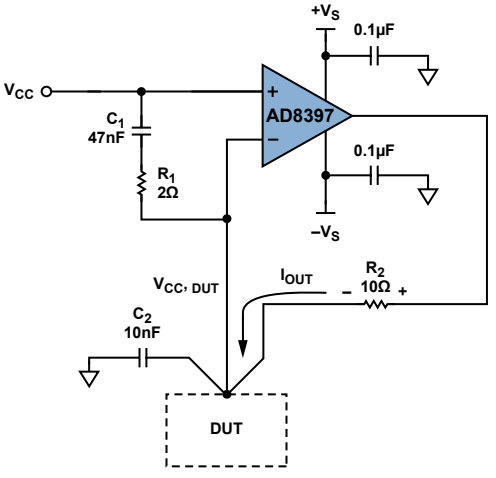

Figure 1. AD8397 as a power supply boost circuit.

Figure 1 shows the circuit that generates the power supply for the device under test (DUT). The AD8397, configured for a closed-loop gain of one, buffers the supply voltage and delivers power to the DUT. Negative feedback and the open-loop gain of the amplifier force the inverting input to be at the same voltage as the noninverting input. If the buffered voltage is much greater than the offset voltage of the op amp over the common-mode range, any errors become negligible. The DUT load current is provided by the AD8397.

The current-sense resistor, R_2, converts the current to a voltage that can be easily measured with an instrumentation amplifier. This sensing technique allows one voltage to be buffered multiple times using separate boost circuits, with each current measured individually. The value of R_2 does not affect the amplifier's dynamic behavior, but it can limit its headroom. Figure 2 shows how the output voltage changes as it drives more current. In this example, the supply voltage is 15 V; R_2 is 10 Ω; and the desired DUT supply voltages are 6 V and 9 V. The graph shows that the circuit saturates at around 650 mA for the 6-V case and at around 500 mA for the 9-V case.

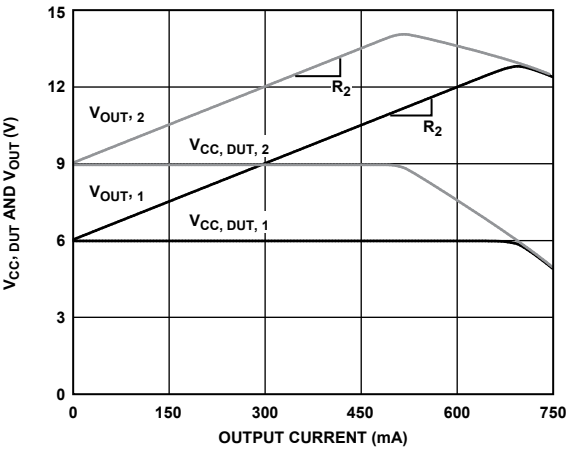

Figure 2. DUT supply voltage and AD8397 output voltage vs. output current.

Keeping resistor R_2 small increases the amplifier's headroom, but a larger resistance helps protect the circuit from accidental current overdrives that could damage the buffer. As the current increases, the amplifier's output voltage goes up until the output saturates or the amplifier becomes damaged. The larger the resistor, the sooner the output saturates, keeping the power dissipation to a manageable level. The amplifier's power dissipation during normal operation must also be considered, as the AD8397 can only drive 750 mA for short periods of time without being damaged.

The buffered DUT supply voltage is decoupled with capacitor C_2. In conjunction with resistor R_2 this capacitor forms a feedback pole that can lead to instability. To fix this problem, the closed-loop gain of the system could be increased, increasing the phase margin and stabilizing the loop, but the magnitude of the voltage that could be buffered would be limited by the output swing.

The network comprising R_1 and C_1 increases the closed-loop gain at high frequencies, while maintaining unity gain at low frequencies. The ratio of R_2 to R_1 defines the high frequency closed-loop gain of the system. The larger the gain, the more stable the system. Capacitor C_1 and resistor R_1 set the frequency where the transition from unity gain to nonunity gain occurs. This corner is set to at least one decade below the crossover frequency of the amplifier to maintain stability.[3] With the values depicted in Figure 1, this boost circuit can drive up to 10 nF loads while maintaining unity-gain stability.

A Kelvin connection can be made by routing the inverting input (sense) and the AD8397 output (force) into the DUT separately, as shown in Figure 1. The output of the amplifier is forced to a voltage that compensates for the resistive loss due to the high current flow in the feedback path. Very little current flows through the sense line, so the inverting input tracks the noninverting input. This technique keeps the voltage on the DUT supply pin at the desired value.

The AD8397 can source and sink current, so it can also be used to generate the negative power supply to a DUT.

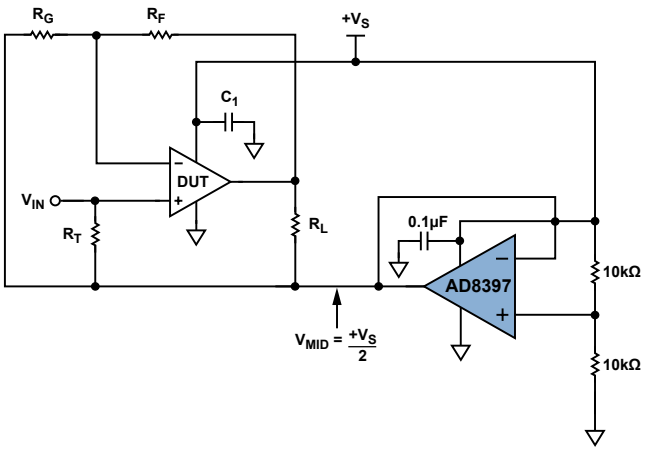

Figure 3. AD8397 as a midsupply reference.

The AD8397 can also act as a midsupply reference voltage for a single-supply DUT, as shown in Figure 3. Here the AD8397 buffers half the supply voltage, as determined by the resistor divider. The amplifier can source and sink current while keeping the midsupply voltage constant. It is essential to operate the AD8397 off of a single supply to obtain bidirectional current. To decouple the midsupply voltage, the same compensation technique previously discussed is necessary. A Kelvin connection and/or current-sense resistor can also be implemented.

References

[1] www.analog.com/en/other-products/automatic-test-equipment/products/index.html.

[2] www.analog.com/en/amplifiers-and-comparators/operational-amplifiers-op-amps/ad8397/products/product.html.

[3] Buxton, Joe, AN-257 Application Note, *Careful Design Tames High Speed Op Amps*.

Analog Microcontroller Forms Heart of Low-Cost, High-Efficiency PA Monitor

By Neil Zhao, Mariah Nie, and Ning Jia

Introduction

In view of the looming global energy crisis and an increasing desire to protect our fragile environment, saving energy is crucial for efficient wireless network operation. The power amplifier (PA) is the core of base stations and repeaters and can account for more than half of their total power consumption. Monitoring and controlling the PA can improve efficiency and reduce operating costs; can maximize output power and achieve the highest possible linearity; and can allow the system operator to discover and solve problems, thus improving reliability and maintainability.

ADI has three options for implementing a PA monitor:[1] a discrete solution, an integrated solution based on the AD7294[2] 12-bit monitor and control system, and an integrated solution based on the ADuC7026 precision analog microcontroller.[3] The discrete solution requires many parts, a complicated PCB layout, and more PCB area, all of which lead to higher cost. The AD7294 has a higher level of integration, lower cost, and higher reliability, but it needs an external microcontroller (MCU) to implement the functions. The ADuC7026 shares many of the benefits of the AD7294, but it includes the MCU. In addition, the ADuC7026 supports external synchronized sampling, which is useful for TD-SCDMA applications.

This article describes a reference design—based on the ADuC7026—that realizes the functions of monitoring and controlling the power amplifier, including configuring the output power, monitoring the voltage standing wave ratio (VSWR), monitoring the laterally diffused metal oxide semiconductor (LDMOS) drain current and temperature, and signaling an alarm when a parameter is over a predefined threshold.

System Block Diagram

Figure 1 shows the block diagram of the PA monitor. The RF signal passes through the voltage-variable attenuator (VVA), the ADL5323 predriver, the power amplifier, and the bidirectional coupler before it is transmitted by antenna. The ADuC7026 MCU samples the temperatures and currents of the two LDMOS stages in the PA module, as well as the forward- and reverse power of the PA module. The MCU sends the sampled data to the PC for display in the user interface (UI). The operator can adjust the system parameters through the UI.

PA Monitor Module

Temperature Monitoring: The power amplifier's power consumption influences its performance. The PA sometimes operates at a high quiescent point but at low output power. Lots of energy is wasted heating the LDMOS devices, thus decreasing their reliability. Monitoring the PA temperature and adjusting its operating point can achieve best system performance.

Figure 2 shows the functional block diagram of the temperature monitor, which uses the ADT75 digital temperature sensor to monitor the temperature of the two LDMOS stages. Available in 8-lead MSOP and SOIC packages, the ADT75 digitizes the temperature to a resolution of 0.0625°C. Its shutdown mode reduces the typical supply current to 3 μA.

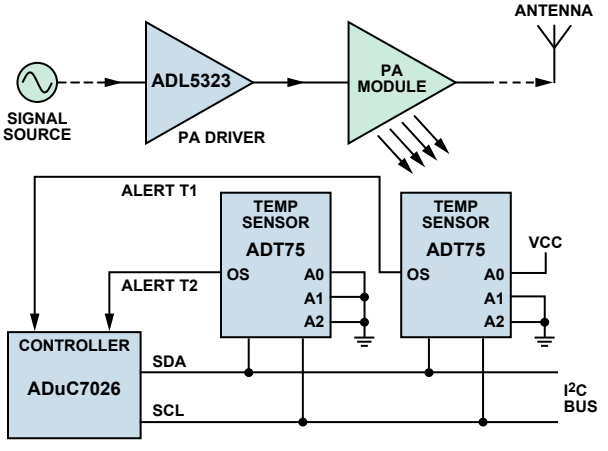

Figure 2. Temperature monitor functional block diagram.

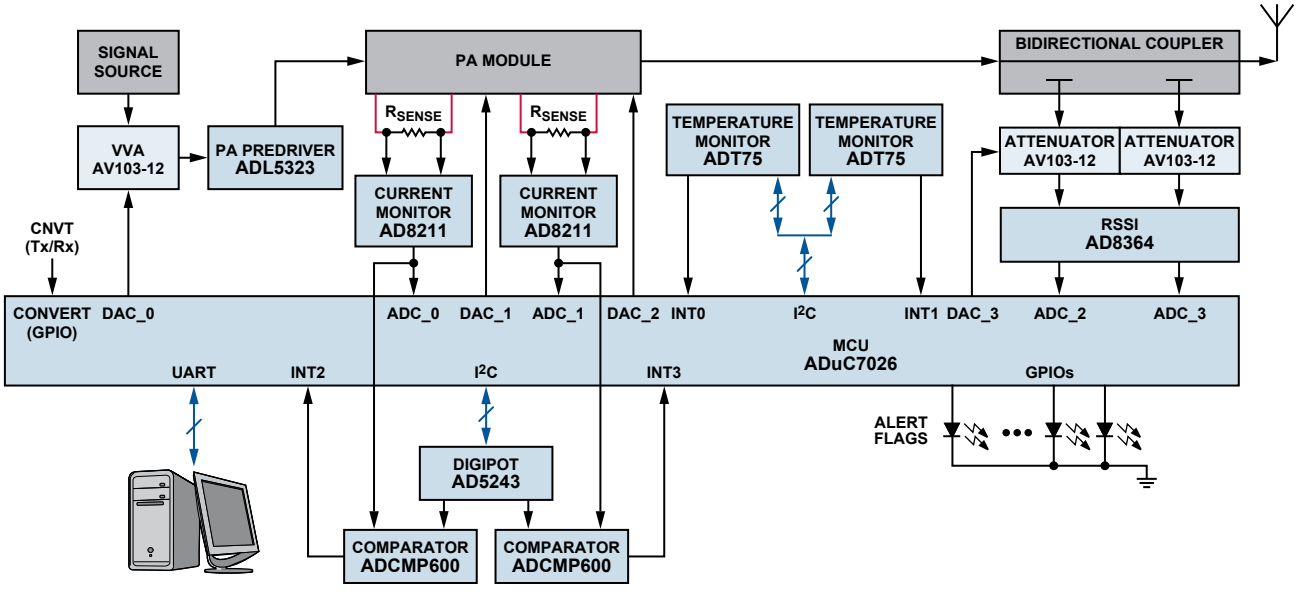

Figure 1. System block diagram.

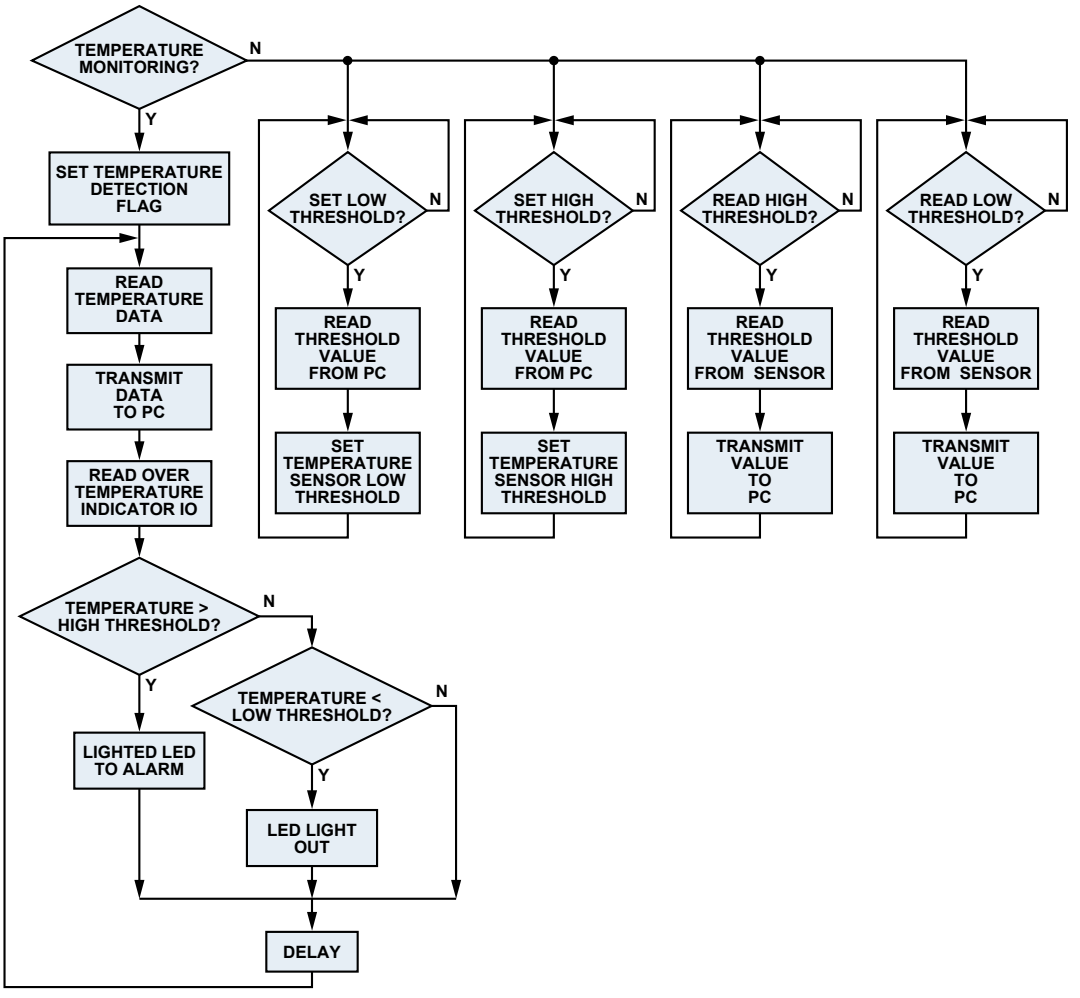

Figure 3. Flow chart for temperature monitoring routine.

Figure 3 shows the flow chart for the temperature monitoring routine. After receiving the temperature detection command, the ADuC7026 MCU sets the temperature detection flag. Next, it reads the temperature data from the ADT75 via the I²C® bus and transmits the data to the PC. Then, it looks at the ADT75's overtemperature pin (OS/ALERT) and turns on an LED if the temperature is over the threshold. If the ADuC7026 receives the configure temperature threshold command, it reads the configuration data from the PC and writes the threshold temperature to the ADT75 via the I²C bus. If the microcontroller receives the read temperature threshold command, it reads the threshold temperature from the ADT75 and transmits it to the PC.

Current Monitoring: The PA performance can be improved by keeping the LDMOS drain current stable over time and temperature; this also maintains the output power in the expected range. The temperature and high-voltage supply influence the drain current; the high-voltage supply also influences the drain voltage. The LDMOS drain current can be measured with a high-voltage current-shunt monitor. If the drain current is continuously monitored, an operator can readjust the gate voltage when a voltage surge occurs on the high-voltage supply to keep the LDMOS working at the best operating point.

Figure 4 shows the functional block diagram of the current monitor, which uses the AD8211 precision high-voltage current-shunt amplifier to sample the drain current of the two LDMOS stages in the PA module. The AD8211 features a fixed gain of 20 V/V, with a typical ±0.5% gain error over the entire temperature range. The buffered output voltage, which directly interfaces with typical analog-to-digital converters, is sampled by the ADuC7026's on-chip ADC. The drain current threshold is set by the AD5243 digital potentiometer, which is controlled by the ADuC7026 via the I²C bus. The output of the ADCMP600 comparator determines when the drain current is over or under the threshold. The system lights the corresponding LED to alert the operator if the drain current is over the threshold.

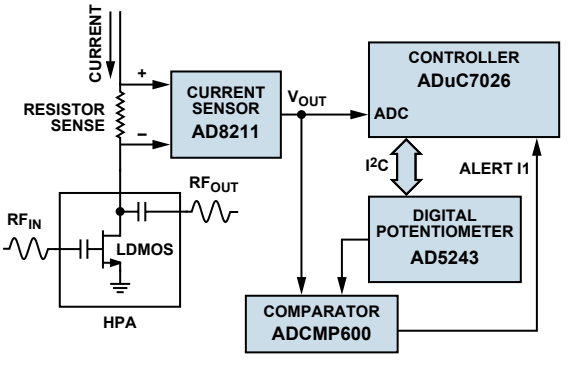

Figure 4. Current monitor functional block diagram.

VSWR Monitoring: VSWR, a key parameter in antenna systems, provides a measure of the match between all of the elements in the antenna system. Reverse power influences the PA's output power, and the transmitted signal is distorted if it is too high. So, it is necessary to monitor VSWR to maintain optimal performance in base stations.

Figure 5 shows the functional block diagram of the VSWR monitor, which uses a bidirectional coupler and the AD8364 dual TruPwr™ detector to measure forward- and reverse power. The AD8364 2-channel, true-rms-responding RF power-measurement subsystem precisely measures and controls the signal power. Its flexibility allows easy monitoring and control of RF power amplifiers, radio transceiver AGC circuits, and other communications systems. The AD8364 output can be used to calculate VSWR and monitor the match on the transmission line. A large VSWR indicates a problem with the antenna, so the operator should protect the system by adjusting the PA gain or the power supply voltage.

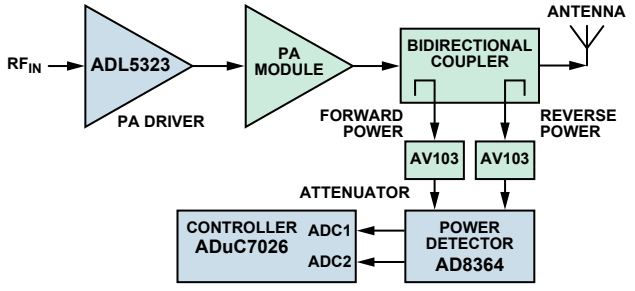

Figure 5. VSWR monitor functional block diagram.

Autopower Control: The transmitter must ensure that the power amplifier can satisfy the system requirements and hold the output power at the desired value—high enough to cover the expected area but low enough to keep from influencing another base station. It should provide overpower protection to ensure that the power amplifier does not operate in an overpower condition, which can cause the power amplifier to saturate and the signal to have nonlinear distortion. For these reasons, the output power must be tested and controlled to make sure it remains steady.

Figure 6 shows the functional block diagram of the autopower control loop, which comprises the bidirectional coupler, TruPwr detector, microcontroller, and voltage-variable attenuator. The bidirectional coupler transfers the forward power to the TruPwr detector, which tracks the change in signal amplitude. The ADuC7026's on-chip ADC samples the output. The microcontroller compares the actual output power with the expected power and uses a proportional-integral-derivative (PID) algorithm to adjust the control voltage error, making the power amplifier operate at the point of best performance.

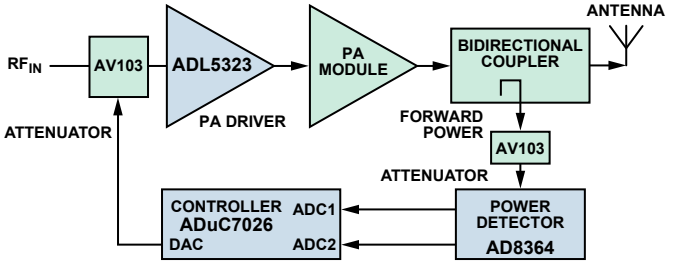

Figure 6. Autopower control functional block diagram.

Figure 7 shows a flow chart for the PID algorithm. First, the program initializes the control parameter K_p, K_i, and K_d and sets the expected output power. Next, the ADC samples the output of the AD8364. The sampled data is then filtered and converted to power. Then, the difference between the expected output power and the actual output power, the next expected sample value, and the control voltage are calculated according to the system transfer function, and the DAC registers are configured. This completes one cycle of the sample and control process, which then continues in a circular manner.

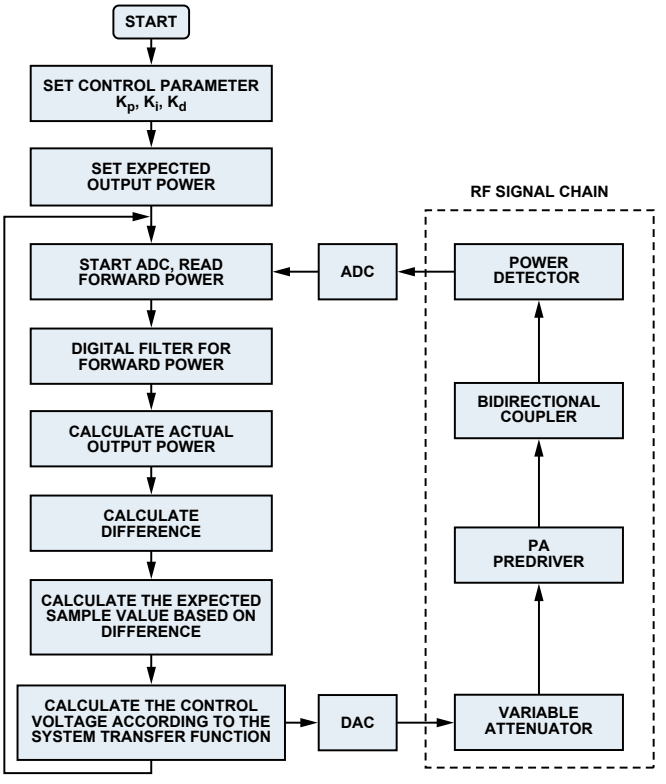

Figure 7. Flow chart for PID algorithm.

User Interface

The user interface (UI) displays the detected data and responds to commands from the operator. Figure 8 shows the flow chart for the UI. The serial port should be opened and communication links should be started after the UI is running. A different module can then be selected for detection and control.

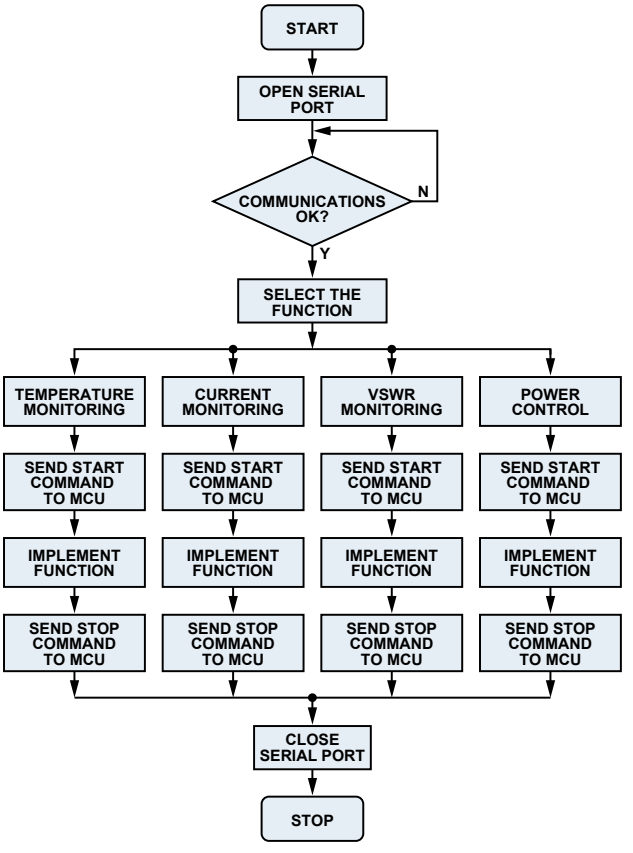

Figure 8. Flow chart for controlling the UI.

Figure 9 shows the temperature test result. A user can change the high- and low-temperature thresholds at any time. In the example, the high threshold is changed from 35°C to 31°C. When the ambient temperature rises above the new threshold, the overtemperature alarm light turns red and the PC sounds a continuous alarm.

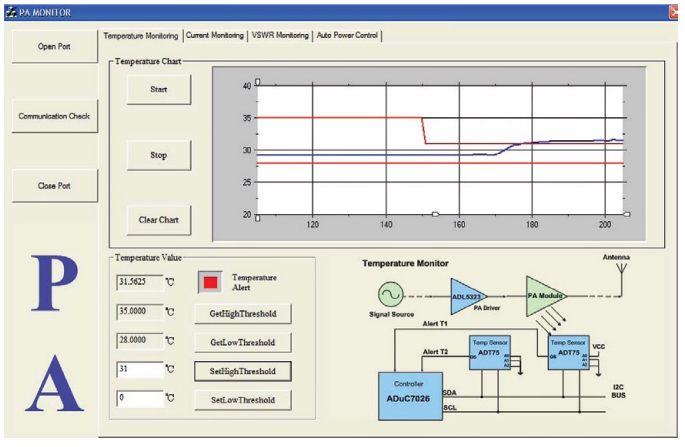

Figure 9. Interface for showing temperature test result.

Hardware Connection

Figure 10 shows the connection of the PA monitor demo. The main board is powered by a 6-V adapter. It connects to the PC with a serial cable so that the lower-end ADuC7026 MCU can communicate with the upper-end PC. The RF signal, generated by the ADF4252 fractional-N PLL synthesizer evaluation board (EVB), is connected with the RF input of the main board. The RF signal proceeds through the signal chain as follows: RF Input→Variable Attenuator→PA Predriver→Bidirectional Coupler→RF Output→Spectrum Analyzer. The output frequency of the ADF4252 EVB is controlled by the PC through a parallel to serial cable.

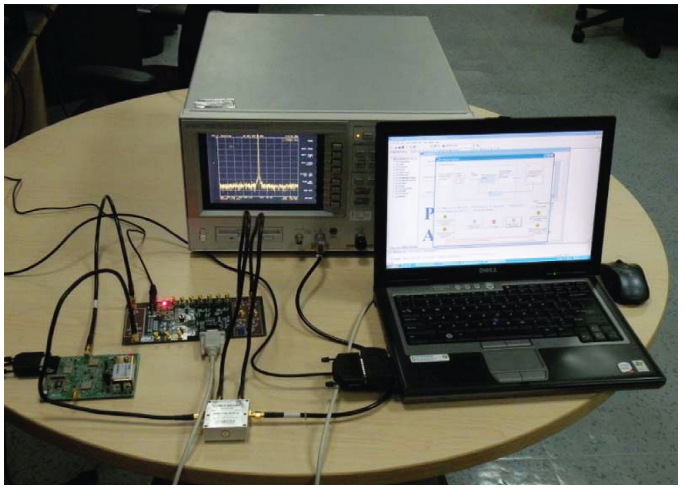

Figure 10. Hardware connection for PA monitor demo.

Conclusion

This reference design provides an integrated solution for monitoring and controlling the PA in cellular base station (GSM, EDGE, UMTS, CDMA, TD-SCDMA), point-to-multipoint, and other RF transmission systems. Using ADI's ADuC7026 precision analog microcontroller to implement the PA monitor application can add flexibility with its multichannel, high-performance 12-bit ADC and DAC, as well as its on-chip programmable logic array (PLA). Conversions can be initiated by the external conversion input or the PLA conversion output. This is helpful for TD-SCDMA applications, which need synchronized signals to sample forward power. The advantage of the integrated PLA is obvious: users can easily and compactly implement logic according to their requirements. Moreover, all kinds of algorithms, such as PID control, VSWR monitor, temperature monitor, and current monitor, can be realized by the ADuC7026, so no other controllers are required. From a system design perspective, this integrated solution can save PCB area, ease PCB layout, decrease system cost, and improve reliability.

Authors

Neil Zhao [neil.zhao@analog.com] has worked as a field applications engineer with the China Applications Support Team at ADI for one year. He provides technical support for horizontal analog products across China. In January 2008, Neil graduated from Beihang University with a master's degree in communications and information systems. He has published several articles.

Mariah Nie [mariah.nie@analog.com] is the manager of the China Applications Support Team. She has worked at ADI for five years and is responsible for supporting horizontal analog products across China. Mariah graduated in 2003 from Beijing Institute of Technology with a master's degree in electrical engineering.

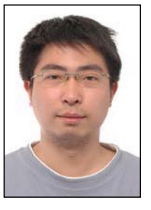

Ning Jia [ning.jia@analog.com] is a field applications engineer with the China Applications Support Team. At ADI for two years, he is responsible for providing technical support for horizontal analog products across China. Ning graduated in 2007 from Beijing University of Posts and Telecommunications with a master's degree in signal and information processing.

References

[1] www.analog.com/library/analogdialogue/archives/42-04/pa_control.html.

[2] Data sheets and additional product information on all ADI products can be found at www.analog.com.

[3] www.analog.com/en/analog-microcontrollers/products/index.html.

Reconstruct a DAC Transfer Function from Its Harmonic Spectral Content

By Ken Gentile

All DACs exhibit some degree of harmonic distortion, which is a measure of how well the DAC reproduces a perfect sinusoid at its output when its input is driven with a numeric sequence representing an ideal uniformly sampled sinusoid. The output spectrum will contain harmonic content due to the DAC's nonideal transient and static behavior. The transient output characteristics of the DAC include slew rate limitations, asymmetrical rise and fall times, and finite settling time. The static characteristics relate to how the transfer function deviates from a straight line. This article focuses on the static behavior and defines a method for deriving the DAC transfer function from the harmonic content observed in the output spectrum. The analysis assumes that the transfer function, rather than the transient output characteristics, is the dominant source of the observed harmonic distortion. This assumption is valid at low frequencies.

The DAC Transfer Function

Figure 1 shows an ideal DAC transfer function, which is the diagonal straight line, $y = mx + b$. The digital inputs reside on the x-axis and the analog output resides on the y-axis.

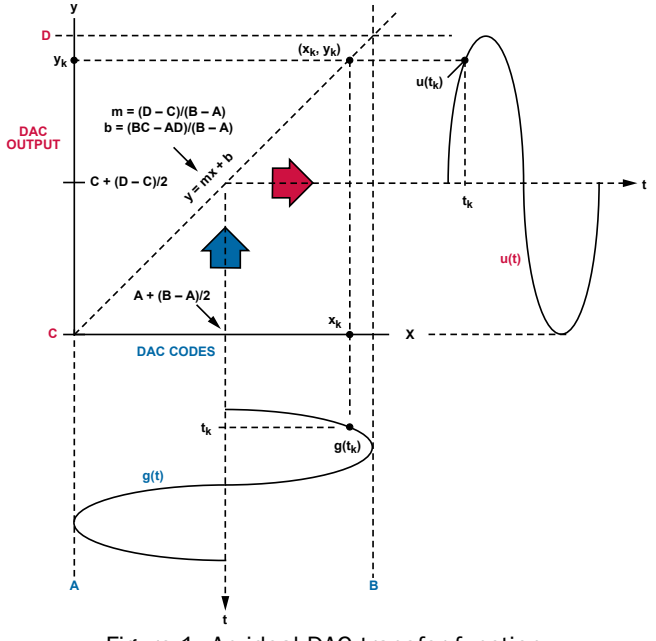

Figure 1. An ideal DAC transfer function.

The range of interest on the x-axis is from the smallest code on the left (A) to the largest code toward the right (B). The range of interest on the y-axis is from the lowest output value at the bottom (C) to the largest output value near the top (D). The equations defining the slope (m) and y-intercept (b) of the ideal transfer function are shown in terms of the boundary values A, B, C, and D. The signal g(t) represents an undistorted sine wave consisting of digital inputs in the range of A and B with time progressing downward. The signal u(t) represents the analog output, which spans values from C to D with time progressing to the right.

The output signal is a reflection of the input signal via the transfer function. Notice that the output signal is the result of linking each point on g(t) to its associated point on u(t). Figure 1 shows an example of the transfer operation at the specific time instant, $t = t_k$, which identifies point $g(t_k)$ on the input signal. The transfer function, in turn, links $g(t_k)$ to the corresponding point, $u(t_k)$, on the output signal. With an ideal linear transfer function, u(t) will be a scaled version of g(t). Note that $g(t_k)$ corresponds to point x_k on the x-axis, which reflects, via the transfer function, to point y_k on the y-axis. Prior knowledge of the coupled sets of points $(g(t_n),u(t_n))$ makes it possible to identify the associated points (Xn, Yn) on the transfer function. Thus, the relationship between points on the input signal, g(t), and points on the output signal, u(t), completely defines the transfer function.

For an N-bit DAC, boundary values A and B take on specific values: namely, $A = 0$ and $B = 2^N - 1$. Boundary values C and D, on the other hand, are conveniently assigned as C = A and D = B. This assignment implies the scale and offset of the actual DAC output signal so that its peak-to-peak span is from 0 to $2^N - 1$. Using these values of A, B, C, and D, the ideal transfer function simplifies to $y = x$ because the slope and intercept become m = 1 and b = 0.

Up to this point, the focus has been on an ideal DAC transfer function, but we now have the tools to deal with a distorted DAC transfer function, $f(x)$, as shown in Figure 2. The main feature to note is that the transfer function is no longer the straight line, $y = x$, but the shaped function, $f(x)$, arbitrarily shown here as a smooth arc. Of equal importance is the effect that $f(x)$ has on the output function, u(t). The ideal input, g(t), reflects off the transfer function, $f(x)$, to produce the distorted output, u(t). The transfer function shown is highly exaggerated compared to that of any off-the-shelf DAC, with the dramatic arc shown for illustrative purposes only. The transfer function of modern DACs barely deviates from the ideal straight line, but even the slightest deviation causes harmonic spurs to appear in the output spectrum.

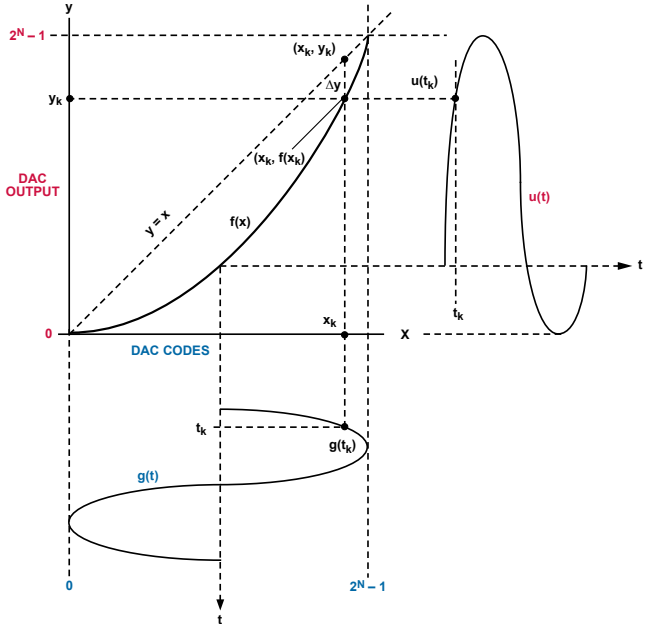

Figure 2. A distorted DAC transfer function.

Successful reconstruction of the DAC transfer function relies on the ability to determine each point, $(x_k,f(x_k))$, from knowledge of g(t) and u(t). This is a two-step process: first, drive the DAC input

with a numeric sequence representing a perfectly sampled sinusoid, measure the DAC output with a spectrum analyzer, and record the magnitudes of the fundamental signal and as many harmonics as possible; then, convert the measured harmonic magnitudes into a transfer function with a specific shape. If done properly, simulating u(t) by passing g(t) through f(*x*) will yield the same harmonic distortion values as those measured.

Step I: Measure the DAC Harmonics

The first step requires an input sequence that represents one cycle of a perfect sinusoid sampled at uniformly spaced time intervals. The goal is to reconstruct the DAC transfer function, so the input signal must contain at least one occurrence of every DAC code from 0 to $2^N - 1$. The input sequence requires more than 2^N samples to exercise every DAC code with equally spaced samples, and it actually takes at least 2^{N+3} samples to guarantee that every code is hit. The following formula produces a perfect sinusoidal sequence of 2^K DAC codes with $K \geq N + 3$. The function, *round*{*x*}, rounds *x* to the nearest integer.

$$g_n = round\left\{\left(\frac{2^N - 1}{2}\right)\left[1 + \sin\left(\frac{2\pi n}{2^K}\right)\right]\right\} \quad (1)$$

where n = 0, 1, 2, 3, ... $2^K - 1$

This equation assumes that the DAC decodes digital input words in straight binary format, as unsigned integers from 0 to $2^N - 1$. For offset binary or twos-complement DACs, g_n must be adjusted to indicate negative values.

The numeric sequence (g_n) is repetitively delivered to the DAC at sample rate f_S, so the DAC output spectrum contains the fundamental signal at frequency $f_O = f_S/2^K$. The harmonics appear at $2f_O$, $3f_O$, $4f_O$, and other integer multiples of f_O. The magnitude of these harmonics is subject to a sin(x)/*x* response due to the sampled nature of the DAC output spectrum. Because f_O is such a small fraction of f_S, however, the sin(*x*)/*x* response is virtually flat and can be ignored. With an 8-bit DAC, for example, $K \geq 11$ and $f_O \leq f_S/2048$, so the sin(*x*)/*x* will be no more than 0.39% (0.034 dB) out to the 100th harmonic.

Accurately reconstructing the transfer function, f(x), requires recording the magnitude of as many harmonics as possible based on a set of harmonic numbers (h). These integers start with h = 1 (the fundamental frequency) and end with h = H, where H is the highest harmonic number for which a measured magnitude is taken. For example, for measurements taken out to the 10th harmonic, H = 10, and the set of harmonic numbers is h = {1, 2, 3, ... 10}

Next, associate the magnitude (M) of each measured harmonic with its harmonic number. For example, M_1 is the magnitude of the 1st harmonic (the fundamental); M_2 is the magnitude of the 2nd harmonic; and so on through M_H. Harmonic magnitudes are usually measured in decibels relative to the magnitude of the fundamental (dBc). Convert dBc to linear units by:

$$M_h = 10^{D/20} \quad (2)$$

where D is the measured harmonic magnitude in dBc. If, for example, the magnitude of the 3rd harmonic is –40 dBc, then the linear magnitude is $M_3 = 10^{-40/20}$, or 0.01. M_1 always equals 1 because the magnitude of the fundamental is 0 dBc, by definition.

Step II: Reconstructing the DAC Transfer Function

The second step of the process involves relating the measured harmonics to the transfer function. The points on f(*x*) depend on the relationship between corresponding points on g(t) and u(t), so the harmonic magnitudes in the frequency domain must first be converted to a time domain representation. Note that g(t) consists of DAC codes that have a one-to-one correspondence with the time points associated with the sinusoidal form of g(t). The DAC codes comprising g(t), thus, relate to the time domain. Furthermore, since u(t) relates to g(t) via f(*x*), and g(t) is a time domain function, then u(t) must be expressed as a time domain function as well. This allows each time point, t_k, in g(t) to be linked to its associated time point in u(t), which is necessary to determine f(*x*) from g(t) and u(t).

Converting the harmonic magnitudes to a time domain representation is challenging because f(*x*) must relate unambiguously to each possible DAC code (0 to $2^N - 1$) in g(t). Since g(t) is a perfect sinusoid, the only way to ensure uniqueness is to limit the range to where the sinusoid is monotonically increasing, as shown in the highlighted section of Figure 3. Without such a limitation, a single point on f(*x*) could map to two points on g(t) and cause ambiguity.

To demonstrate such ambiguity, imagine sliding region T downward. The point (x_k, f(x_k)) on f(*x*) could now be associated with two points on g(t), an unacceptable occurrence. By limiting the range of T to that shown, ambiguity cannot exist. Because g(t) is a sinusoid, the desired range of T corresponds to ½ cycle with an initial phase offset of 3π/2 radians.

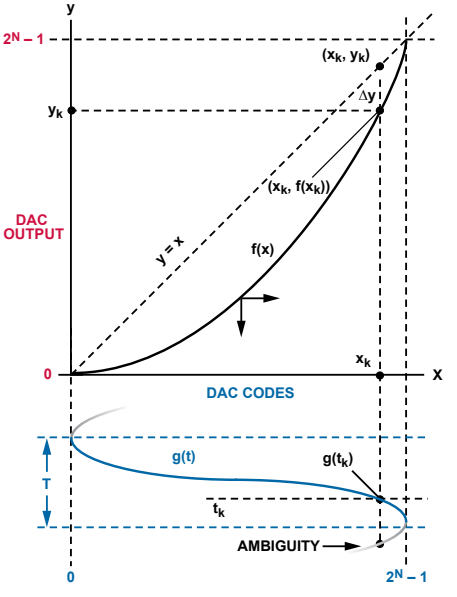

Figure 3. Relationship between f(x) and g(t).

The fact that g(t) is bounded by T implies a similar bound on u(t). Hence, the conversion of the recorded harmonic magnitudes to the time domain must ensure confinement of u(t) to the same range of T as g(t), as shown in Figure 4.

Note that the actual time span, T, is irrelevant because f(*x*) serves only to translate between the amplitudes of g(t) and u(t). To simplify the analysis, normalize the fundamental frequency (f_O) to 1. The frequency of the 2nd harmonic is, therefore, 2; the frequency of the 3rd harmonic is 3; and so on. As a result,

the harmonic frequency is identical to the harmonic number (h): $f_h = h$. This convenient relationship simplifies the mathematics used to create u(t) from the harmonic measurements, M_h.

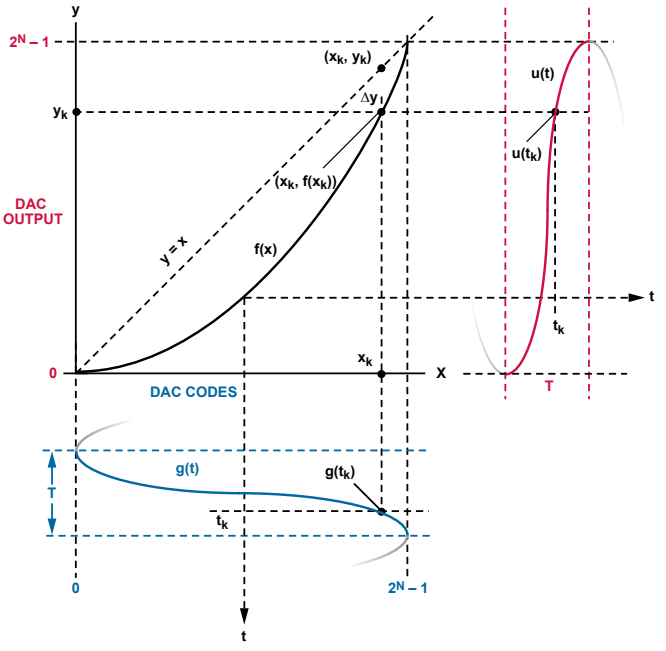

Figure 4. Time domain range of g(t) and u(t).

The general time domain representation of a sine wave is:

$$y(t) = \beta \sin(2\pi ft + \theta) \quad (3)$$

where β is peak amplitude; θ is initial phase offset.

The time domain representation of each harmonic, $u_h(t)$, can be realized by substituting h for f and M_h for β. Recall, however, that g(t) is offset by 3π/2 radians. Furthermore, the link between g(t) and u(t) via f(x) implies that g(t) and u(t) be aligned in phase. Substituting 3π/2 for θ provides the required alignment. In the following equation, note that $0 \le t < 1$ and π replaces 2π to limit the fundamental to a half cycle as indicated by interval T:

$$u_h(t) = M_h \sin\left(\pi ht + \frac{3\pi}{2}\right) \quad (4)$$

With knowledge of the time domain representation of each harmonic, $u_h(t)$, it is possible to reconstruct the composite output, u(t), as the sum of the fundamental and harmonic signals:

$$u(t) = \sum_{h=1}^{H} u_h(t) = \sum_{h=1}^{H} M_h \sin\left(\pi ht + \frac{3\pi}{2}\right) \quad (5)$$

Recall that the goal is to reconstruct the DAC transfer function, f(x), by relating g(t) and u(t). Furthermore, g(t) must consist of exactly 2^N samples in order to maintain a one-to-one correspondence with the points on f(*x*). Hence, calculate the samples of g(t) as:

$$g_n = round\left\{\left(\frac{2^N - 1}{2}\right)\left[1 + \sin\left(\frac{\pi n}{2^N} + \frac{3\pi}{2}\right)\right]\right\} \quad (6)$$

$$(n = 0, 1, 2, 3 \ldots 2^N - 1)$$

Since g(t) consists of 2N samples, it seems reasonable to reconstruct f(*x*) from a u(t) sample set consisting of 2^N samples. It turns out, however, that at least 2^{N+3} samples are necessary to provide suitable accuracy for small values of Mh. With this in mind, calculate each sample of u(t) as follows:

$$u_n = \sum_{h=1}^{H} M_h \sin\left(\frac{\pi hn}{2^{N+3}} + \frac{3\pi}{2}\right) \quad (n = 0, 1, 2, 3 \ldots 2^{N+3} - 1) \quad (7)$$

Note that this results in u(t) containing more samples than g(t). This complicates the mapping of u(t) and g(t) onto f(x) because multiple samples of u(t) can correspond to a single point on f(x) and g(t). Hence, specific groups of samples must be averaged to provide a reasonable mapping onto f(x). The following pseudo-code demonstrates the required mapping assuming an N-bit DAC, 2^N points of g(t), and 2^{N+3} points of u(t). The array, DacXfr, consists of 2^N elements, which are initially zero. After executing the code, the elements of the DacXfr array contain the normalized DAC transfer function.

```
n = 0
FOR i = 0 TO 2^N-1
  AvgCnt = 0
  WHILE i = g[n]
    AvgCnt = AvgCnt + 1
    DacXfr[i] = DacXfr[i] + u[n]
    n = n + 1
    IF n >= 2^N+3
       EXIT WHILE
    END IF
  END WHILE
  IF AvgCnt = 0
    EXIT (fail because array, g[ ], is
    missing a DAC code)
  END IF
  DacXfr[i] = (DacXfr[i]/AvgCnt)/2^N
END FOR
```

Validation

To validate the methods described in this article, a spectrum analyzer was used to measure the output of a 14-bit DAC driven by an input sequence representing a perfect sinusoid. The magnitudes of the first 14 harmonics (Numbers 2 through 15, in units of dBc) were recorded, and the values were used to reconstruct the DAC transfer function, f(*x*). Next, a simulation produced an output sequence, u(t), by passing an ideal sinusoidal input sequence, g(t), through the reconstructed DAC transfer function, f(*x*). An FFT converted u(t) to its frequency domain equivalent, U(ω). The harmonic magnitudes were extracted from U(ω) and compared to the spectrum analyzer measurements, as shown in the tabulated results of Table 1. Note that the largest error, associated with the 7th harmonic, is only 0.065 dB.

Table 1

Harmonic Number	Measured Magnitude (dBc)	Simulated Magnitude (dBc)	Deviation (dB)
1	0.00	0.00	0.000
2	–75.1	–75.100	0.000
3	–74.5	–74.502	–0.002
4	–90.5	–90.501	–0.001
5	–86.5	–86.498	0.002
6	–92.0	–91.999	0.001
7	–95.5	–95.565	–0.065
8	–93.8	–93.801	–0.001
9	–97.2	–97.187	0.013
10	–89.6	–89.599	0.001
11	–94.2	–94.204	–0.004
12	–98.8	–98.802	–0.002
13	–95.6	–95.649	–0.049
14	–99.3	–99.298	0.002
15	–91.1	–91.080	0.020

Due to the scale, a plot of the reconstructed transfer function appears as a straight line ($y = x$). In fact, the transfer function actually deviates from $y = x$ enough to produce the harmonic content shown in Table 1. It helps to plot only the deviation of the transfer function from the ideal straight line, as shown in Figure 5. The vertical axis is in units of LSBs.

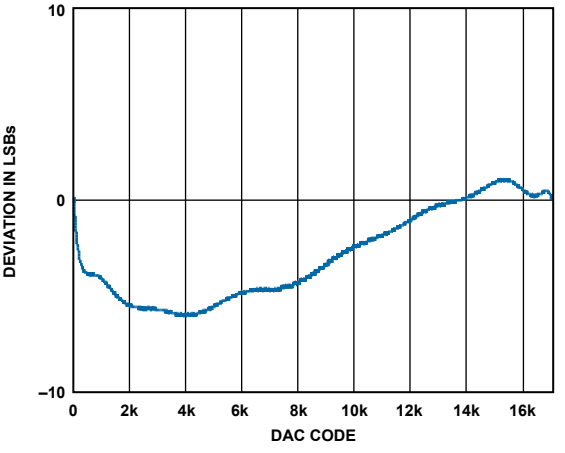

Figure 5. Residual error of DAC transfer function.

Notch Filter Reduces Amplifier Peaking and Increases Gain Flatness

By Charly El-Khoury

The ADA4817[1] *FastFET*™ op amp achieves 1-GHz bandwidth with only 4-nV/√Hz input noise, making it the fastest, lowest noise amplifier in its class. Although the ADA4817 is unity-gain stable, a high-frequency pole increases its gain-bandwidth product from 410 MHz at high gains to 1 GHz at unity gain. Unfortunately, this pole decreases the phase margin, causing unwanted peaking in the frequency response and ringing in the step response. Adding a discrete RLC notch filter to the amplifier's noninverting input maintains the high bandwidth and input impedance, while dramatically reducing peaking, increasing gain flatness, and reducing overshoot.

The RLC notch filter, shown in Figure 1, takes advantage of the amplifier's input characteristics to produce the desired outcome. The notch formed by *R* in parallel with the series *LC* can be shaped to compensate for the peaking produced by the amplifier and the parasitic capacitance. The result, with the values shown, is 1-GHz bandwidth (−3 dB), 250-MHz gain flatness (0.1 dB), and less than 1-dB peaking for a gain equal to 1.

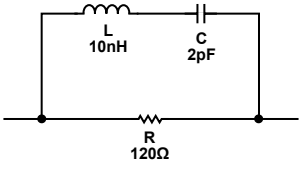

Figure 1. RLC notch filter.

The choice of resistor, capacitor, and inductor is critical. The input impedance of the ADA4817 looks like a 1.4-pF capacitor to ground. Figure 2 shows the *RLC* circuit with the input impedance of the amplifier. This circuit will be analyzed in depth to generate the transfer function $\frac{V_{OUT}}{V_{IN}}$.

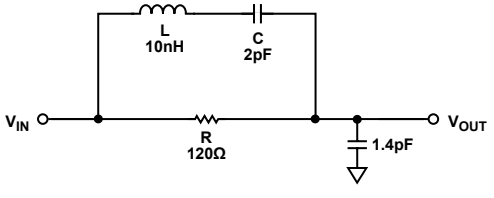

Figure 2. Notch filter and amplifier input impedance.

$$\frac{V_{OUT}}{V_{IN}} = \frac{Z_{C_1}}{Z_{C_1} + Z_R \,||\, (Z_C + Z_L)} \quad (1)$$

Substituting $Z_C = 1/j\omega c$, $Z_L = j\omega L$, and $Z_R = R$, and solving for the magnitude, yields:

$$\left|\frac{V_{OUT}}{V_{IN}}\right| = \sqrt{\frac{C^2R^2\omega^2 + (CL\omega^2 - 1)^2}{R^2\omega^2(C^2C_1^2L^2\omega^4 - 2(C + C_1)CC_1L\omega^2 + C^2 + 2CC_1 + C_1^2) + (CL\omega^2 - 1)^2}} \quad (2)$$

Where C_1 is the amplifier's input impedance and $\omega = 2\pi f$. Figure 3 shows the magnitude response using Equation 2 with $C_1 = 1.4$ pF. The values of *L* and *C* determine where the transfer function crosses 0 dB. The value of *R* determines the depth of the notch.

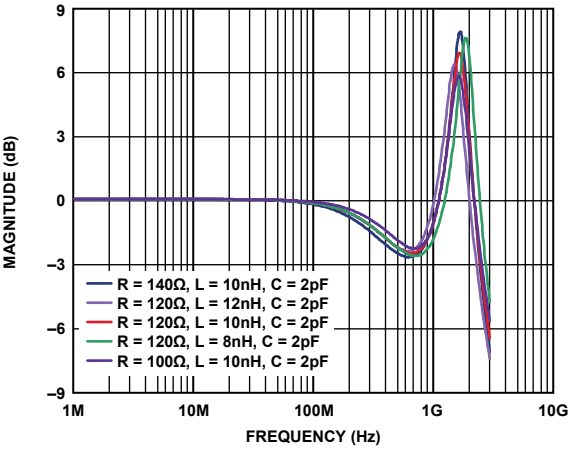

Figure 3. Various RLC notches.

To compensate for the amplifier's peaking, add the individual frequency responses of the amplifier and the filter, adjusting *R*, *L*, and *C* for the flattest overall response. This can be done with Excel or most circuit simulation software. The notch can be shaped to reduce peaking, increase flatness, and reduce overshoot. Figure 4 shows the overall design, where the notch is connected to the noninverting input.

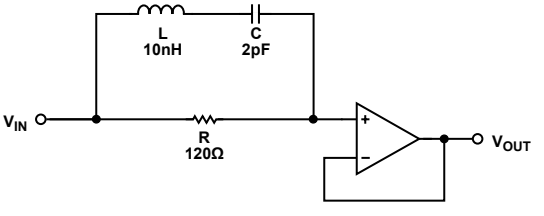

Figure 4. Overall circuit.

Perhaps the most important feature of the FET-input ADA4817 is its extraordinarily low input bias current. The notch circuit maintains this characteristic while preserving the amplifier's low distortion and noise. Figure 5 shows the frequency response of the ADA4817 with and without a notch filter. Note that bandwidth is maintained while flatness is extended and peaking is reduced.

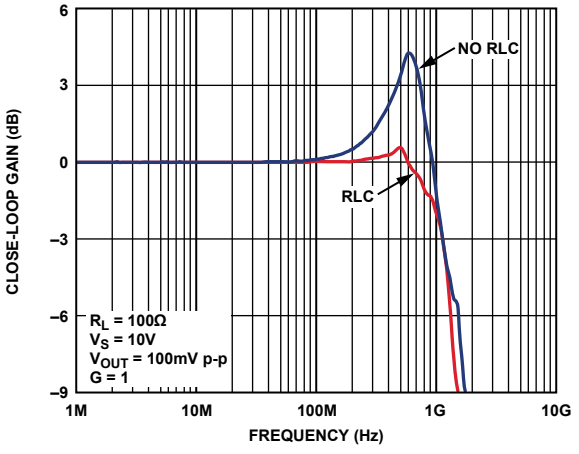

Figure 5. With and without RLC.

Figure 6 shows the step response of the ADA4817 with and without the *RLC* circuit. The same design can also be used to shape the frequency response of other FET-input amplifiers. This design maintains the high input impedance of the FET input, but an *RLC* to ground can be used with amplifiers where this is not a requirement.

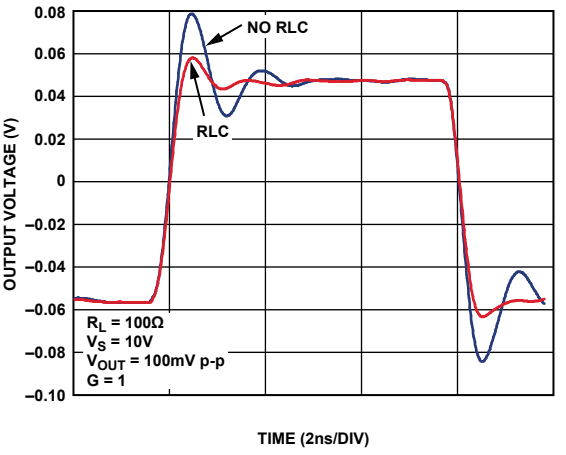

Figure 6. Pulse response with and without RLC.

Conclusion

Adding a discrete RLC notch filter in front of the ADA4817 FET-input op amp dramatically increases its performance. This novel, yet simple, technique decreases peaking, increases gain flatness, and reduces overshoot—all while maintaining the original 1-GHz bandwidth (–3 dB). This robust, inexpensive solution adds three new components, but the additional cost may be worth it if flat frequency response, lower overshoot, and enhanced performance are important.

References

[1] www.analog.com/en/amplifiers-and-comparators/operational-amplifiers-op-amps/ada4817-1/products/product.

This *Should* Work: Thermistor Senses Liquid Levels

By John Wynne

In precision temperature measurement[1] applications using thermistors, RTDs, or other resistive temperature sensors, care must be taken to avoid errors due to self-heating of the sensor by the excitation current. In some applications, however, the self-heating effect can be put to good use. The following design concept *should* work, but it has not been fully tested.

When a thermistor is driven by a voltage source, it heats up. If submerged in a cooler liquid, its temperature and, therefore, its resistance will remain relatively constant—as long as the liquid temperature remains relatively constant. If the liquid level drops, however, the thermistor becomes exposed; the heat dissipating effect of the liquid vanishes; the temperature rises; and—for a positive-TC element—the resistance increases. This can be easily detected and flagged by the ADM4850[2] low-cost half-duplex differential line transceiver. The differential outputs are useful when the level-alert signal must be transmitted to remote annunciators such as LEDs. The transceiver's prime use is in multipoint data communications, so its outputs provide short-circuit protection, thermal shutdown, and slew-rate limiting to reduce EMI.

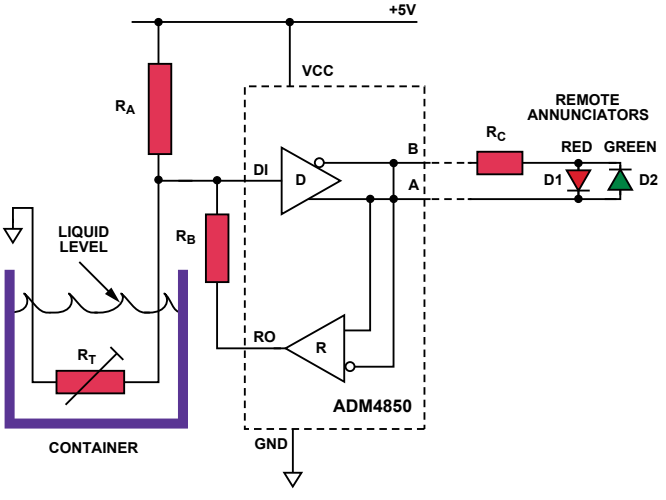

Figure 1. Thermistor senses when liquid is above or below a preset threshold.

We want to know when the liquid in a container is above or below a specific level. As shown in Figure 1, a thermistor is positioned at this level. When submerged, the thermistor resistance is relatively low. The ratio R_t/R_A is chosen so that the voltage at the driver input is interpreted as Logic 0. When the thermistor is uncovered, the input voltage increases rapidly, crosses the input threshold voltage, and is interpreted as Logic 1. The receiver output can be tied to the driver input through resistor RB if hysteresis is required.

Reliable operation of this circuit depends on the input threshold stability—which is not specified on the data sheet—and on the voltage excursions produced by R_t and R_A as the critical liquid level is crossed. Characterization data for the ADM4850—over a number of lots, a 4.75-V to 5.25-V power-supply range, and a –40°C to +85°C temperature range—shows that an input voltage ≤ 1.15 V will be seen as Logic 0 and that an input voltage ≥ 1.42 V will be seen as Logic 1. The thermistor suggested for this application—an EPCOS type D1010[3] ceramic PTC device intended for use as a level sensor—offers a resistance that tracks closely with the thermal conductivity of the ambient medium. The R/T curve for this thermistor type rises extremely steeply once the threshold temperature has been reached. Available in a stainless steel case, it is corrosion-proof to fuels, solvents, and other liquids found in harsh environments.

The value of RA depends on the temperature of the liquid and the surrounding air. The worst-case conditions occur when the liquid is hot and the air is cold. From the D1010 data sheet, a standard value of 909 Ω for R_A is a good choice to operate in liquids up to +50°C and air down to –25°C. Samples of the D1010 measure approximately 149 Ω at room temperature with no excitation.

In industrial applications, a fault might expose R_A or R_t to a lethal high voltage. In these cases, consider the ADM2483[4] transceiver, an isolated version of the ADM4850. This half-duplex differential bus transceiver integrates galvanic isolation that can withstand 2.5 kV rms for 1 minute. An isolated power supply is required to drive the hot side of this device.

References

[1] www.analog.com/en/temperature-control-and-conditioning/functions/index.html.

[2] www.analog.com/en/interface/lvds/adm4850/products/product.html.

[3] www.epcos.com/inf/55/db/ptc_06/Sensors__B59010__D1010.pdf.

[4] www.analog.com/en/interface/digital-isolators/adm2483/products/product.html.

Analog Devices, Inc.
Worldwide Headquarters
Analog Devices, Inc.
One Technology Way
P.O. Box 9106
Norwood, MA 02062-9106
U.S.A.
Tel: 781.329.4700
(800.262.5643,
U.S.A. only)
Fax: 781.461.3113

Analog Devices, Inc.
Europe Headquarters
Analog Devices, Inc.
Wilhelm-Wagenfeld-Str. 6
80807 Munich
Germany
Tel: 49.89.76903.0
Fax: 49.89.76903.157

Analog Devices, Inc.
Japan Headquarters
Analog Devices, KK
New Pier Takeshiba
South Tower Building
1-16-1 Kaigan, Minato-ku,
Tokyo, 105-6891
Japan
Tel: 813.5402.8200
Fax: 813.5402.1064

Analog Devices, Inc.
Southeast Asia
Headquarters
Analog Devices
22/F One Corporate Avenue
222 Hu Bin Road
Shanghai, 200021
China
Tel: 86.21.2320.8000
Fax: 86.21.2320.8222

Printed in the U.S.A. M02000431-x-5/10

www.analog.com/analogdialogue

ANALOG DEVICES